ABSTRACT

Title of thesis: IN-SITU CONFORMAL 3D PRINTING FOR TARGETED REPAIRS

Team PRINT: Rohith Chintala, Brendan Cutick, Tyler Han, Elizabeth Myers, Eric Oh, Aidan Sandman-Long, Cynthia Sheng, Nathan Spicer-Davis

Thesis directed by: Dr. Steven Mitchell
Department of Mechanical Engineering

David Edelen
Chief Engineer Additive Manufacturing KAIROS, Inc

Additive manufacturing is an emerging technology whose users seek to benefit from repair methods to reduce time and material costs. We explored an application of this technology for targeted repairs, such as mending holes or cracks, on 3D printed parts. Using conformal tool-pathing, we combined the precision of additive manufacturing with the strength and homogeneity of material adhesion to repair damage. To characterize the efficacy of targeted 3D printing repair for Fused Filament Fabrication (FFF) plastics, repair configurations varying in shape, size, material, infill and loading type were tested in 3-point bending for structural strength and strain. We provided and summarized the collected data in addition to a structural analysis and optimization of parameters relevant to reparative 3D printing. The collected data found that 3D printed repairs were effective in replacing the strength properties of a damaged area through the use of conformal 3D printing.

Team PRINT Thesis

by

Team PRINT

Rohith Chintala, Brendan Cutick, Tyler Han, Elizabeth Myers, Eric Oh, Aidan Sandman-Long, Cynthia Sheng, Nathan Spicer-Davis

Thesis submitted in partial fulfillment of the requirements of the Gemstone Honors Program, University of Maryland, 2022

Committee:
Dr. Steven Mitchell
David Edelen
Dr. Andrew C. Becnel
Dr. Mark D. Fuge
Dr. Isabel Lloyd
Dr. Ho Yeung

Acknowledgements

Team PRINT would like to thank our mentor Dr. Steven Mitchell for his continued support and guidance as well as David Edelen for his expertise in our research. Thank you also to our former librarian, Dr. Sarah Over, for her help in our literature review and thesis writing process. We would like to acknowledge our discussants for taking the time to read our thesis and provide valuable feedback. We are grateful to current and former Gemstone Staff – Dr. David Lovell, Dr. Vicki Hill, Ms. Jalah Townsend, Dr. Frank Coale, Dr. Kristan Skendall, Dr. Leah Tobin, and Ms. Jessica Lee – for giving our team the opportunity and support to engage in extensive research during our undergraduate years. Finally, we would like to pay our gratitude to the team's family and friends for their continuous support.

Table of Contents

Figure List

Chapter 1: Introduction

In order to produce a component for any project, there are currently two methods of production: additive and subtractive manufacturing. Additive Manufacturing (AM) is the process of depositing material in predefined locations to create a structure. 3D printing is a popular example of AM. There seems to be few limits to the possibilities of additive manufacturing in mechanical design and manufacturing. In addition to producing scale models and rapid prototyping, AM is capable of making complex, functional, and durable structures. For example, rocket nozzles capable of withstanding the high pressures and thermal stresses of rocket propulsion [1]. Industries are taking seriously the engineering applications of 3D printed structures in their products: a 3D printed airplane structure was subjected to representative loads applied to the fuselage and wings [2]. Both of these developments demonstrate that AM can be used in high-stress applications and that there is a trend in trying to replace current manufacturing techniques with lower cost, light-weight AM materials and processes. Given that 3D printed structures are likely to become increasingly common and used for crucial components in a variety of complex systems, we believe it is necessary to investigate how the operational lifetimes of such components can be extended and material waste can be minimized so that this relatively new technology can be used as responsibly as possible.

In mechanical structures, frequently used components will gradually wear over time. A component such as the interface for a motor shaft is critical to the operation of the greater mechanism but even superficial damages can render it useless (e.g. stripped locking grooves). Once the damage is severe enough, a typical solution is to replace the component entirely. Depending on the size of the component and the severity of the damage, this can be very wasteful in terms of the materials and time needed to reprint and replace the damaged component.

Some applications may not even have the option of replacing damaged components, such as in the aerospace industry. Damage to rover wheels has been cited as a reason for being unable to complete mission objectives and limiting the areas that are accessible to the rover [3]. With no replacement parts, no accessible servicing stations, and no way to return the rover to Earth, the system simply must be able to endure whatever damage it may experience. Similarly, the design lifetime of a satellite takes into account the rate of damage it is expected to experience from micro-meteoroids and other orbital debris.

It would be far more advantageous if a repair was applied directly to the damaged parts, preserving structural integrity and shape to enable continued use. While one can approach direct repair using either subtractive or additive methods, several industries such as those in aeronautics or astronautics have directed attention towards additive manufacturing, taking advantage of AM's quick and cheap prototyping. Thus, it would be desirable to have an additive repair method which aligned with the interests of these industries. Having the ability to repair damaged components using AM could drastically increase a system's lifetime, and even allow for an entirely more efficient design.

In our review of the existing literature, we found that AM for in-situ repairs has not yet been thoroughly investigated. This poses several potential questions and criticisms which should be answered before proceeding with such technology: Can a repair effectively reinstate a component's viability of operation? Is the repair worth the time and material costs? Under what circumstances can a component be repaired? Clearly, the answers to these questions will vary by application. In the following work, we choose to investigate Fused Filament Fabrication (FFF) parts. FFF parts are widespread in both hobbyist and engineering industries. Plastics like Polylactic Acid (PLA) are commonly used in prototypes and engineering drafts. In addition, considering the resources available to us, proceeding with FFF and plastics (as opposed to metal fabrication methods like Selective Laser Sintering) present the most feasible option while permitting proof-of-concept experiments.

In an attempt to quantify a repair's structural integrity, the experiments (discussed further in Chapter 3) include three-point bending of repaired structures while varying properties of print such as infill percentage, infill pattern, and plastic material. By thoroughly collecting and analyzing data, we will be able to give unambiguous answers to the above questions and identify new questions that we believe would be worth investigating in the future. We are particularly interested in optimization of targeted 3D printed repairs, and our work suggests that there exist parameters which improve structural strength and efficiency which are not immediately intuitive.

The following chapter will delve deeply into the background of the problem and provide context for our proposed solution. After that, a discussion of the methodology used will provide full detail of our experimentation, data collection, and data analysis methods as well as the motivation behind them. Following the methodology, we will present and discuss our results, and in doing so, we will answer the questions we have identified as being relevant to determining whether our proposed repair method is "effective." Finally, we will end with a discussion of what future research we recommend be done in order to build off of our work and progress further towards an implementable solution.

Chapter 2: Literature Review

2.1 Introduction and Applications

The following literature review presents a survey of recent or related research that aids the development of an in situ 3D printer. The full implementation of such a device is needed in order to make repairs to structures that are in unsafe or inaccessible environments for humans. Repairs for on-orbit satellites and extraterrestrial rovers are applications where the technology will be invaluable. Historically, rovers have experienced physical damage that has compromised abilities to fully complete missions [4]. This includes wheel damage that has restricted mission sites to relatively flat terrain [4]. In figure 1, the wheel thickness is 0.75mm and the approximate diameter of the hole is 3cm. Voids on the scales of 1cm - 5cm would be ideal for this application. It would be possible for a 3D printer to attach to a robotic arm and navigate to the desired location for reparative printing. Implementation of a robotic arm capable of these wheel repairs aligns with NASA's efforts [5] toward the potential of sending multiple small and collaborative rovers on missions. In this situation, it is plausible for there to be a robot specifically designed to repair other rovers in situ to aid in lengthening future missions and mitigating unforeseen damage.

Figure 1. Image from MastCam of Mars Curiosity Wheel Damage. Image: NASA [6]

A specific example of reparative 3D printing was recently tested by Saab AB, a Swedish aerospace company, in March 2021. The company tested how additive manufacturing could be applied to a damaged component of their aircraft in a simulated battlefield setting [7]. They achieved this by removing a panel from their aircraft, scanning the void, and 3D printing an exact replica of the missing piece using a nylon PA2200 polymer [7]. Since there was no 3D model of the aircraft piece, it had to be scanned. In real life, damage to aircrafts will be unpredictable, so it is important that there exists a way to model this. Applications for this type of repair include rapid repairs for jet aircraft that have sustained damage during missions in remote locations. A 3D printed piece, using a suitable material for the application, could save time on readiness.

The results of this test were successful. Saab found no visible structural damage after the test flight, which has positive implications for this field [7]. Saab is currently investigating more effective material choices that have greater flexibility and temperature resistance; however, the Nylon PA2200 was able to withstand flight conditions.

In the following sections, we discuss literature related to the aspects of the project that require immediate attention for implementation. This includes the materials in question, the slicing and gcode required to print our specimen, and existing work regarding infill patterns.

2.2 Materials

For the purpose of our project, we will be testing our in situ repairs using PLA and ABS filament. These materials are inexpensive compared to other popular filaments and compatible with the Ender 3 Pro. This section discusses and compares the physical properties and applications of these two filaments.

2.2.1 PLA

Polylactic acid (PLA) is a common filament used for 3D printing due to its high strength and low cost of $20-$30/ per kilogram [8]. It is one of the world's most researched 3D printed materials and has proven applications in bio-printing, rapid manufacturing, construction and home development, and more.

Although PLA has a tensile strength of 59 MPa and an elastic modulus of 3500 MPa, it is a very brittle material. PLA exhibits 5-7% elongation at break, according to researchers at MIT [8]. Furthermore, it has poor heat resistance properties. This limits its applications to those that do not require plastic deformation at high-stress levels or extreme temperature ranges.

Despite these downsides , PLA is actively used in the medical field. Specific applications in this area range from 3D printing stents and screws in surgery to soft-tissue implants and tissue engineering scaffolds [8]. Another set of MIT researchers, Shady Farah and Daniel Anderson, analyzed the mechanical properties of PLA and their functions in everyday applications. They looked at how PLA is used in the medical field and what considerations are needed when selecting a filament. Farah and Anderson cite that properties such as flexural modulus, tensile strength, and elongation are all critical criteria to consider when using PLA [8].

2.2.2 ABS

Acrylonitrile Butadiene Styrene (ABS) is another common filament used in FFF printing. ABS has high impact strength and a working temperature range of -30 Celsius to +60 Celsius, so it can be used in extreme temperature environments [9]. According to researchers at Omnexus, ABS can withstand up to a maximum of 50% elongation at break, which characterizes ABS as a relatively ductile material in FFF printing [9].

One of the most common applications of ABS is in piping systems. The polymer can endure long-term heat exposure with relatively small changes to its physical properties, making it suitable for a variety of fluid temperatures [10]. Another benefit of this filament is abrasion and chemical resistance. It is very chemically resistant to aqueous acids and can withstand corrosive environments [10]. Specifically, in gravity flow piping systems, the abrasion resistance enables long-term low surface roughness. This leads to a slope reduction in the piping and can reduce building height and cost [10]. In some cases, ABS pipes are favored over stainless steel because of these factors.

2.2.3 Comparison of Filament Properties

Researchers at the University of Manchester subjected five common FFF filaments to a three-point bending test. Their results show that PLA is 77% stronger than ABS in this type of environment [11]. Our project aims to build off of this research by using a three-point bend test to determine the strength of various infill patterns and infill percentage combinations of a repaired specimen. The bar graph below shows the flexural modulus for PLA, ABS, and their different carbon fiber variations. Reinforcing filaments with carbon fiber is known to increase the strength of the material [11]. Although we did not test carbon-fiber reinforced PLA (CFR-PLA) in our research, it is important to note for future applications.

2.3 Slicing

2.3.1 Direct-Print Process

Some challenges facing conformal additive manufacturing are related to material properties and the algorithm used to generate the toolpath. For 3D planar printing, a filament is deposited in the x-y plane within the same layer with a constant z-value in layer with an amount equal to the desired layer thickness. 3D conformal printing brings more challenges in this printing method in that the z-value changes dynamically with the x-y values within the same layer according to the shape of the print base. In response to these challenges, Alkladi et al [12] came up with a tested and working algorithm specifically for conformally printing on uneven surfaces.

In the workflow, the most important step that sets the difference between conformal and planar 3D printing is step 2 where the offset of the freeform substrate to be used as a slicing surface is determined. A gap height (the distance between the printing substrate and the nozzle tip) is one of the main factors that has a direct influence on the filament shape and printing quality. In planar 3D printing, this can be set by moving the substrate vertically by an H amount (where H = layer thickness x layer number) [12]. However, for conformal printing, the gap height should be fixed according to the normal of the surface of the freeform substrate. Thus the H amount in this case is set to equal to the desired gap height so that the distance between the middle of the nozzle tip and the surface of the freeform substrate will be constant throughout the whole layer.

A few key points of this algorithm aside for the consideration of the gap height is the toolpath generation for each layer which is composed of perimeters and infill data points. The perimeter data points are extracted from the intersection between the 3D model and the slicing surface, while the infill data points are the result of the projection of the 2D pattern on the slicing surface [12]. The limitation on this algorithm is described to be a 45 degree maximum inclination agle between the nozzle and the freeform substrate when using a Cartesian system with only three degrees of freedom.

2.3.2 Adaptive slicing and curved-layer toolpathing

Another type of additive manufacturing process is the layer-based process. However, the method poses a number of set-backs with its stair-stepping surface including aesthetic perception as well as mechanical properties. An attempt to mitigate the effects of stair-stepping include one made by Ahlers et al in which the nonplanar printing method is explored and solved [13]. In the implementation proposed by Ahlers et al, the identification of printable surfaces poses to be one the biggest features in which the algorithm must have.

The general idea of Ahlers et al implementation of the nonplanar toolpath generation is that nonplanar layers replace regular ones at the top of printed objects and all other regions are sliced and printed with the regular planar slicing implementation. The regions that are nonplanar printable are moved to the highest possible layer and get warped down onto their intended position after the toolpath generation [13]. In their research, three aspects were used to the print: layer generation, toolpath generation, and collision avoidance. First, the object model must be sliced into horizontal slices that are usually evenly distributed along the z-axis of the printed object. For each layer, multiple polygons are generated that represent the outline of the layer. In these slices, the areas where nonplanar layers should be printed are also identified and are then later lifted to the highest layer.

After the slicing comes the toolpath generation that starts with using the standard planar perimeter and surface filling algorithms are used to fill the planar layers with planar toolpaths. Then the three-dimensional tool path is generated out of the previously created two-dimensional toolpath by projecting down every extrusion path that lays on a layer with an attached nonplanar surface. The extrusion paths are generated out of multiple two-dimensional points and then adding a z-component to each point of the path. Lastly, the intersections of an extrusion line with all facets calculated in planar two-dimensional space and new points are inserted and projected to the correct z-height at each intersection. These final nonplanar layers are illustrated in Figure 2.

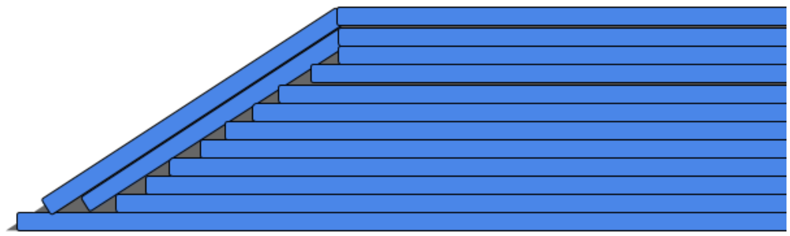

Figure 2. Nonplanar Layered Print Cross Section

The G-code created by Ahlers et al [13] also includes collision checks for the layers. For planar areas on higher layers, the intersection of a collider polygon and the current layer polygon is calculated starting from the bottommost layer. If the intersection is not empty, then there is a collision. If it is, then the intersection is added to the collider. Then this collider is offset by the width that the collision model would gain within one layer height. This new extended collider is then used for the collision check on the next layer above. When all layers are collision free, the whole extrusion path of this nonplanar layer is collision-free within the current object. Another factor that is accounted for in collisions is traveling from or to a point that lies below the highest printed layer. But that is also solved with the printhead lifted to the current maximum printing height between points.

2.4 Existing Work regarding Infill Patterns

2.4.1 Optimal Print Settings

In order to maximize the durability of our repaired parts, it is beneficial to have the optimal print settings for our tests. Researchers at the University of Manchester conducted a study to find the optimal modeling parameters for FDM printing using pure PLA filament. They varied the infill pattern, infill density, infill speed, and nozzle temperature. The researchers analyzed the data using a combination of tensile and compression testing, as well as scanning electron microscopy (SEM) to reach a conclusive set of optimal printing parameters [11]. Their findings showed that a linear infill pattern, 100% infill density, 90mm/s infill speed, and 215 degrees Celsius nozzle temperature were most effective for maximizing the Young's Modulus of PLA 3D printed parts under tension and compression loadings. The maximum Young's Modulus the researchers recorded for PLA was 1538 MPa [11].

Tanner Harpool, a thesis candidate at Wichita State University, also investigated the effects of infill patterns on tensile strength properties of 3D printed parts. He analyzed three different types of infill patterns: rectilinear, diamond, hexagonal. Harpool found that the hexagonal pattern had the highest tensile strength. Harpool also noticed that prints with 100% infill behaved like brittle materials, which actually decreased their strength. Parts with a lower infill percentage experienced behavior more closely resembling a ductile material [12].

Another important aspect to consider in this project is the adhesion between the base part and the infill repair. In the study mentioned above, the researchers used SEM technology to reveal that the strength of the samples is dependent on the arrangement of their layers [11]. This justifies it is worthwhile to pursue the optimal infill pattern for 3D printed repairs because the orientation and layout of the filament along the 3D printed base will most likely have an effect on the overall strength of the repaired piece.

There is some correlation between these parameters. For example, researchers found that increasing the nozzle temperature leads to an increase in strength; however, at a certain point, the increase in temperature becomes detrimental [11]. If the temperature is too high, it can lead to poor layer bonding, which does more harm than good. It is important to note that the change in one parameter may have an adverse effect on another parameter. In our case, we are varying the infill pattern and infill density of our repaired print. By varying the infill pattern, we may also alter the adhesion between the filament layers, and this is something that needs to be noted during data analysis.

Researchers from the University of Malaysia Perlis did further research into both the tensile and flexural strength of 3D printed parts [15]. They tested various infill patterns and compared their ultimate strengths from tensile and flexural tests. This testing found that the rectilinear infill pattern yielded the highest flexural and tensile strength followed by the hexagonal, aligned and hilbert curve patterns [15].

2.4.2 Structural Analysis

Existing research on structural analysis of 3D printed parts focuses on either tensile or flexural testing. For 3D printed parts, to compare different printing parameters, researchers have used tensile and flexural tests detailed in the ASTM D638-14 and ASTM D790-10 standards. The goals of the ASTM D638-14 and ASTM D790-10 are to test the tensile and flexural properties of plastics respectively. The ASTM D790-10 standard details a 3 point bending test on a given specimen. The test requires a span to depth ratio of 16:1 and for the test to continue until the part breaks or the specimen reaches 5% strain. This test also requires at least 5 specimens for a given combination of parameters to ensure proper results. To calculate the flexural strength

$$\sigma_f = \frac{3PL}{2bd^2} \qquad \text{Equation 1.}$$

σ_f = Flexural Strength

P = Load [N]
L = Support Span [mm]
b = width of beam [mm]
d = depth of beam [mm]

from the force measured during the test, the equation 1 was used where P is the load, L is the support span, b is the width of the specimen and d is the depth of the specimen. The standard defines the midspan deflection with equation 2 where r is the strain.

$$D = \frac{rL^2}{6d} \qquad \text{Equation 2.}$$

D = maximum deflection at center of beam [mm]

The flexural strain is defined as equation 3 where D is the maximum deflection.

The modulus of elasticity was defined by equation 4 where m is the slope of the initial line of the load-deflection curve.

$$\varepsilon_f = \frac{6Dd}{L^2} \qquad \text{Equation 3.}$$

ε_f = Flexural Strain [mm/mm]

$$E_B = \frac{L^3 m}{4bd^3} \qquad \text{Equation 4.}$$

E_B = Modulus of Elasticity in Bending [MPa]
m = slope of tangent to initial line of the load-deflection curve [N/mm]

Of these calculations detailed in the ASTM standard, the most commonly used metric for comparing different parameters was the ultimate strength of the printed part. The ultimate strength is the maximum stress the specimen experiences as it undergoes the test. With common specimen designs, this metric allows a direct comparison between different parameters to find optimal conditions. Because of this, ultimate strength is measured and compared while doing structural analysis of 3D printed parts.

2.4.3 Cost Analysis

Researchers at the department of mechanical and industrial engineering at Youngstown State University investigated the relationship between infill print design and production cost-time of 3D printed ABS parts. This relationship is extremely important to consider in our research because while users would want to select the infill print pattern that provides them with the best strength retention, they also need to review production costs associated with each infill pattern. Selection of an infill pattern can significantly affect mechanical properties, total cost, and production time .

The researchers printed multiple specimens of four different infill patterns: low density, high density, double dense, and solid infill. The prints were subject to ASTM standards, which are the same standards we are using in this project. Once printed, the researchers tested the tensile, compressive, and bending strength of each infill pattern. To calculate the total cost of each print, they estimated the cost per minute of printing ABS on their print setup, then multiplied this by the time it took to print the sample . Certain infill patterns will contain more material, which leads to higher costs; furthermore, the toolpath the extruder head takes for complex infill patterns can also increase the print time. These are all factors that need to be accounted for in a cost-benefit analysis. In a practical cost-benefit analysis, the situation is everything. For a Mars Rover, the extra cost associated with a stronger repaired piece may be well worth it. On the other hand, in a mass production application, the cost would likely be the driving factor.

The Youngstown State University researchers found that in order to obtain a greater cost reduction, the user should expect a decrease in the mechanical strength. However, the data shows that although the low density piece had a very similar modulus (MPa) to the high density piece in bending tests, the low density piece had much better cost savings when compared to the solid infill piece. The low density had a modulus of 456.68 MPa, while the high density piece had a modulus of 459.83 MPa. The cost savings of the low density infill when compared to the solid piece was close to 4%, and it actually cost 3.5% more to print the high density infill piece. The researchers suggest additional analysis on more complex infill patterns [3].

Chapter 3: Methodology

3.1 Background and Reasoning

3.1.1 Background

Upon building the printers and 3D printing preset models, the team moved into creating a procedure and establishing standards for printing pieces. Beginning with a layer height of 0.2 mm (the standard layer height for a 0.4 mm extruder head) and a 20% infill, the team initially ran into problems with layer separation. This is caused by a lack of adhesion between two layers in a print that results in a slight gap which can compromise the structural integrity of the piece. To remedy this issue, the layer height was adjusted to 0.12 mm. After finalizing the layer height, the infill percentage was increased to 100%, since this would be the maximum infill used throughout our trials. While testing this, a common issue the team faced was warping. The temperature of the bed is controlled and held constant during the printing process by the printer itself. For PLA this temperature was 70 degrees Celsius. The temperature of the PLA is controlled as it leaves the extruder, however, any plastic not in direct contact with the bed cools down and therefore contracts. This can result in deforming near the bottom of the print which compromises its structural integrity. To combat this problem, the printers were insulated using cardboard, all windows in the printing room were closed to prevent drafts, and hairspray was used on the print bed to keep the print attached to it. After these modifications, the team had great success with printing pieces similar to that of our damaged pieces and began our specimen testing. Using a separate model for the infill piece, the 3D printer successfully printed in the hole to repair it. The progression of these results is shown in the figure below.

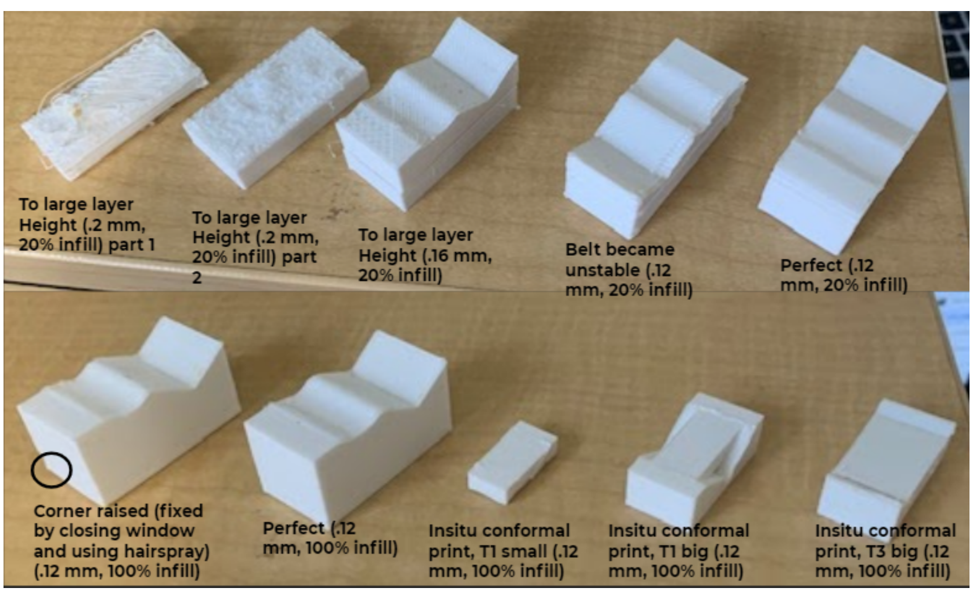

Figure 3. Progression of initial prints

3.1.2 Reasoning

One of the main objectives of our research was to determine the most efficient infill pattern and infill percentage combination for repairing a damaged 3D printed part. Efficiency in our case is defined as the strength of the repaired piece over the time it took to repair the damaged section.

$$Repair\ Efficiency = \frac{Maximum\ load\ (kg)}{Print\ time\ (sec)}$$

The team chose to print the test specimens as rectangular beams for simplicity and easier data analysis. Printing in this configuration allowed for multiple variations of the simulated damage section. The main simulated damage section used, denoted as T1 was an inverted triangular prism which is shown below in figure 4a. Our secondary simulated damaged section, denoted at T4 was a semispherical void which is shown below in figure 4b. The specimens comply with common practice ASTM standards, which are discussed further in section 3.3.

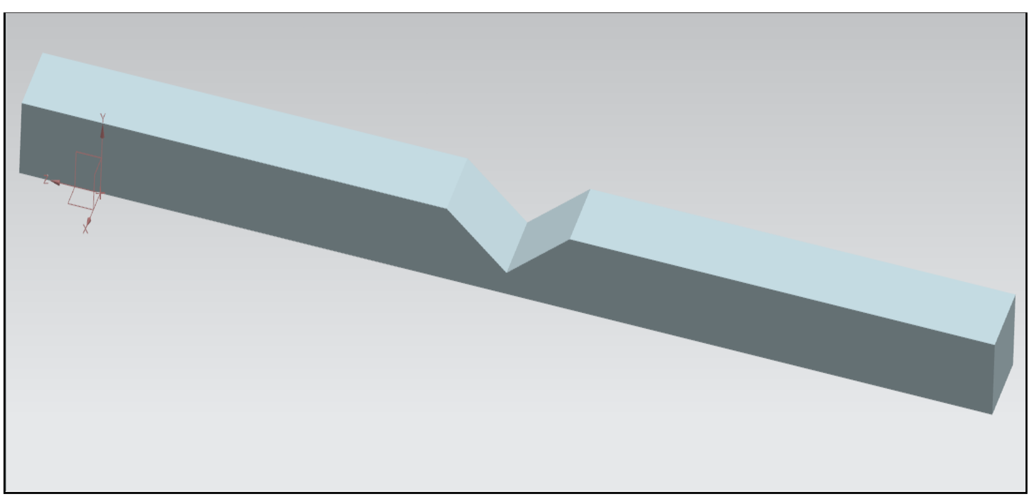

Figure 4a. T1 damaged specimen without repair

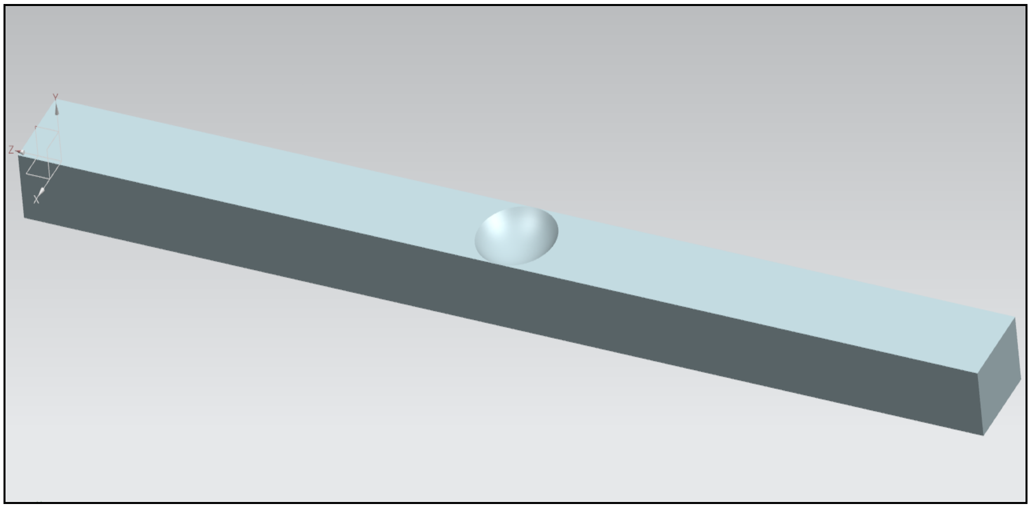

Figure 4b. T4 damaged specimen without repair

The voids were chosen as a proof of concept for the ability to repair two completely different types of damage. Due to limitations with the dimensions of the nozzle used, the maximum angle that the 3D printer could print on was 45 degrees above the horizontal. As a result, the voids chosen could not at any point require printing on a surface above 45 degrees as demonstrated in figure 5 below.

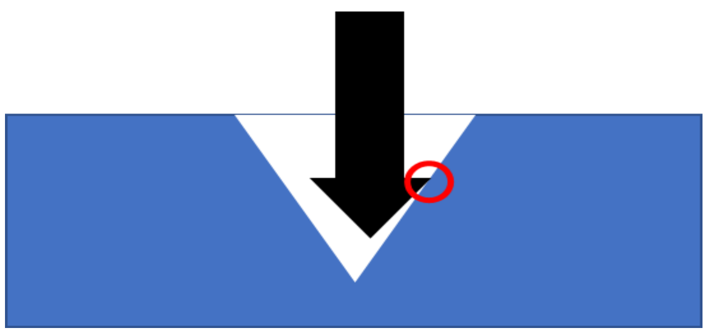

Figure 5. Justification of 45 degree limitation

The T1 and T4 void geometries were selected to mimic simplistic slice and circular imprint damages while also meeting the angle requirements. In addition, additively repairing a component may first require using subtractive methods to get a relatively smooth and regularly shaped void to print into, which could very likely be similar to the T1 and T4 shapes.

The team determined the best method to evaluate the strength of a repaired piece was a 3-point bend test. This test is one of the most commonly used tests for collecting stress versus strain data for a structure, and was abundant in the literature related to our project. It is known for its ease of specimen preparation and testing. Another common method to collect stress versus strain data is a tensile strength test; however, due to the testing equipment available to us (more detail on test apparatus in section 3.4.2) a 3-point bend test was easier to perform than a tensile test, and either would have been able to give us sufficient information.

3.2 Hypothesis(es)

The goal of this research was to test whether a damaged 3D printed structure could be repaired using conformal printing methods in such a way that the strength of the structure post-repair would be within 80-100% of the strength of the original undamaged structure. The team predicted that the design and settings of the printed repairs could be varied in order to maximize the strength of the repaired structure and achieve the ultimate strength of an undamaged piece.

As discussed in section 3.1, we developed designs for two different types of damage that we could repair and test. Along with these different types of damage, the main focus of our research analyzed two factors: infill percentage and infill pattern. In order to find the optimal infill percentage, we conducted tests with 20%, 40%, 60%, 80%, and 100% infill. Researchers in Switzerland conducted tensile testing to compare 3D printed pieces with 20%, 50%, and 80%

infill and found 80% to have the greatest tensile strength, so we predicted that an infill percentage of 80% would yield the strongest repair during our testing [16]. To vary the infill pattern, we conducted repairs using the rectilinear, hexagonal, and aligned infill patterns. Figure 6 below provides a visual comparison of the infill patterns where the positive x direction is the axial direction along the test piece. According to a study conducted at the University Malaysia Perlis, the rectilinear pattern displayed the highest tensile strength when compared to more complex infill patterns such as hexagonal and aligned, so we determined that rectilinear would likely be the strongest in our experiment [15].

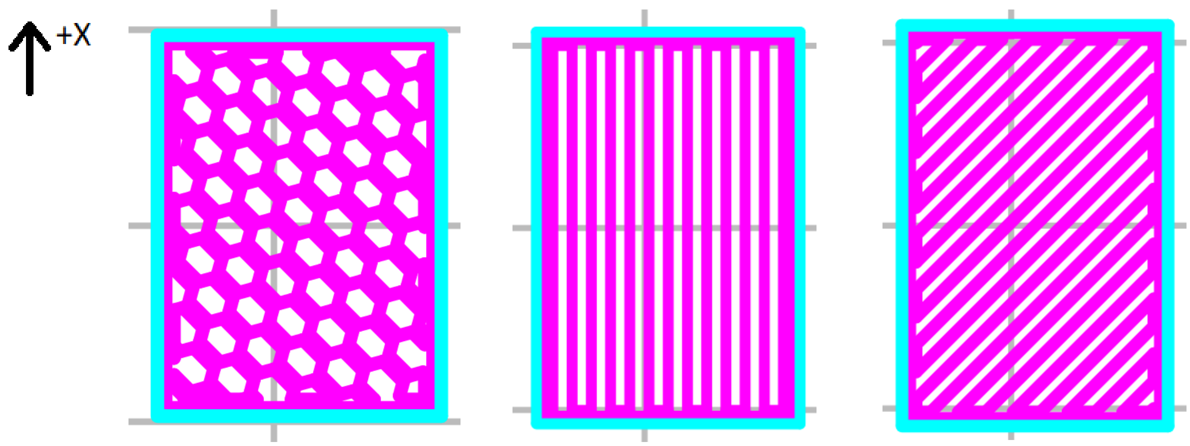

Figure 6. Different infill patterns. From left to right: Hexagonal, aligned, rectilinear

Although our project focused solely on conducting 3D printed repairs using fused filament fabrication (FFF), we believe that the methods we developed and tested could be modified and applied to other types of 3D printing as well in future studies.

3.3 Testing Standards

For the experimentation process, we adhered to the ASTM D790 standard for testing the tensile properties of plastics. These standards determined the overall dimensions of our printed pieces and the number of pieces to be tested for each category. ASTM requires 5 parts to be tested for each variable, so we chose to print and test 6 pieces for each type of infill percentage and pattern in order to be more thorough [17]. We also used this standard to determine the dimensions of the printed test pieces. The requirements for bend testing of plastic parts included a 16:1 span to depth ratio for each design. In addition, each end needed to have an overhang length that was 10% of the span when mounted in the testing setup [17]. As a result, each of our pieces was 19.2 cm long with a 1cm depth and 1.5cm width.

The standards we used to determine these dimensions were intended for rectangular plastic test pieces. For the purpose of our study, we used rectangular prisms with designed damage as shown in section 3.1.2. As shown in figures 4 and 5, these pieces were not precisely rectangular due to the repaired damage, but the overall designs were approximate rectangular prisms so we chose to use these standards for all experiments.

3.4 Materials & Equipment

3.4.1 Printer

To print all specified pieces, four Ender 3 Pro 3D printers were purchased. The printers were assembled, operated, and housed by team members. The Ender 3 Pro was purchased because it is inexpensive, easy to operate, and has a sufficiently-sized print bed. Four printers were needed in order to accommodate the large number of pieces required.

In addition to the variables outlined above, several rounds of testing were conducted with pieces made out of acrylonitrile butadiene styrene (ABS) plastic, another commonly used material in FDM additive manufacturing other than PLA. The purpose of testing other materials was to determine whether our results were specific to PLA, or if there is reason to believe they are applicable to FDM in general.

The Ender 3 Pro used a 0.4mm nozzle with a layer height of 0.12mm. The printer bed (dimensions of 220 x 220 x 250 mm) was set at 70℃ for 1.75mm PLA filament and 95℃ for 1.75mm ABS filament. The nozzle was set at 200℃ for both filaments. Speed, acceleration, and jerk speed were kept at standard settings to maintain consistency across all printers. A picture of the set up is shown below in figure 19.

3.4.2 Testing Equipment

The team initially planned on utilizing equipment available on the University of Maryland campus to perform 3-point bend tests and collect data. Due to the COVID-19 pandemic this was no longer an option. To ensure that we would be able to continue collecting data regardless of pandemic procedures, we decided to construct our own testing/data collection apparatus that would remain in and be operated from our own homes.

To perform 3-point bend tests, we used a Mophorn 6 ton H-frame hydraulic shop press. This is a hand-operated press that works by pumping a lever to generate a load on the specimen.

A load cell measured the force applied by the press and was attached using J-B Weld cold-steel epoxy. We considered other types of presses such as more expensive models with built-in load cells and electronic actuators. There were two reasons why we chose the simpler, hand-operated press. The first was budgetary constraints. A higher-end model would have taken up the majority of our budget, leaving little room for printers and other supplies. By building our own testing apparatus with the simpler press, we were not only able to have multiple test setups, but also allocate more of the budget for printers and printing materials. This proved to be incredibly helpful as the time required to print and test all of the samples was a significant constraint. The other reason for choosing the simpler press was for the learning value of the experience. While not related to the empirical results of this study, we believe that the process of designing and fabricating our own testing apparatus provided us with valuable experience in engineering, design, and troubleshooting. This also allowed us to become more familiar with the standards and methods for testing in 3-point bending, giving us a better understanding of the procedures involved in testing and analyzing the results.

In addition to the press itself, the test pieces were supported by two steel plates on either end which were clamped to the frame of the press. The steel plates also needed to be raised a few centimeters so that the pieces had room to be bent to failure. To do this, steel hex bolts were placed under the corners of each steel plate. At the edge of each steel plate and on the bottom of the load cell are ¼" diameter stainless steel D-shafts with the flat sides attached with epoxy to the plates and load cell respectively. This was to make sure that all the forces applied to the test piece were each being applied at a single point to allow for easier and more accurate structural analysis. The end supports were positioned 16 cm apart, with the load cell midway between.

Figure 7. Testing Apparatus

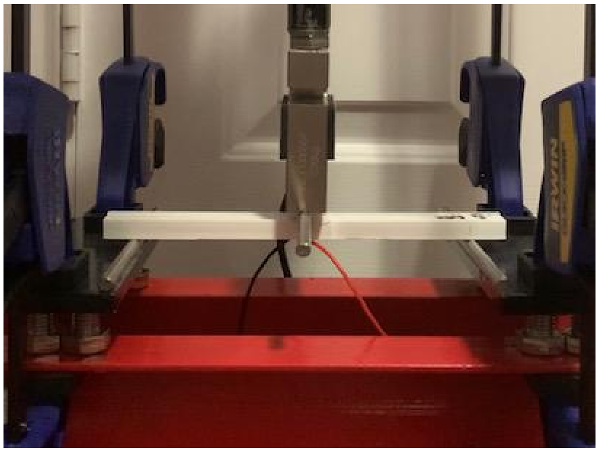

Figure 8. Test piece positioning

Data collection was performed using an Arduino Uno microcontroller, a 200kg S-type load cell, and 350-ohm resistance strain gauges. The load cell was wired to the Arduino with an HX711 load cell amplifier, and could measure the applied force directly. To measure strain, the strain gauge was set up in a Wheatstone bridge circuit with three other resistors as in the figure below. A Wheatstone bridge is used for sensing strain by detecting small changes in voltage across the resistors corresponding to changes in resistance of the strain gauge. The Wheatstone bridge was also connected to the Arduino via an HX711 load cell amplifier. Figure 9 below is a diagram of the circuit we used to take data.

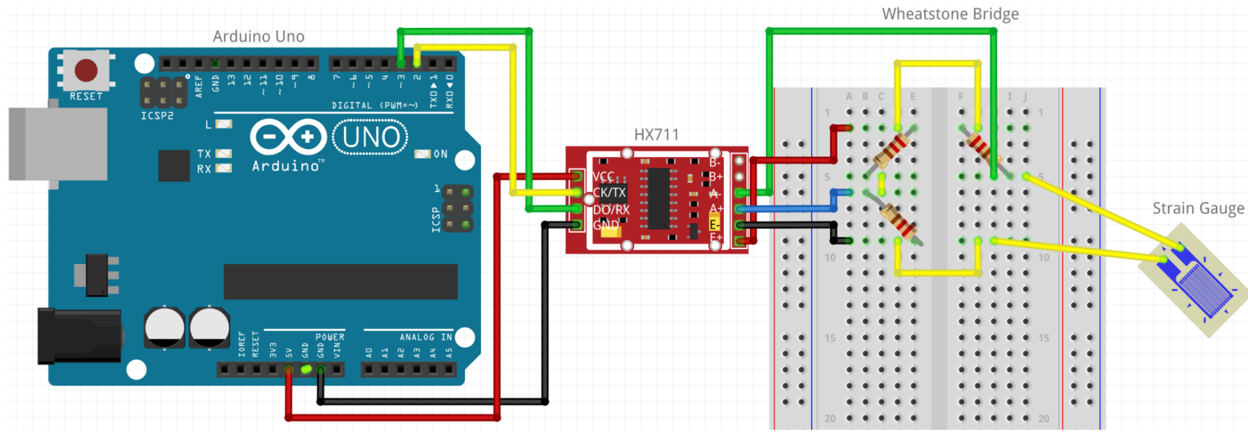

Figure 9. Wheatstone bridge, HX711, and Arduino circuit diagram

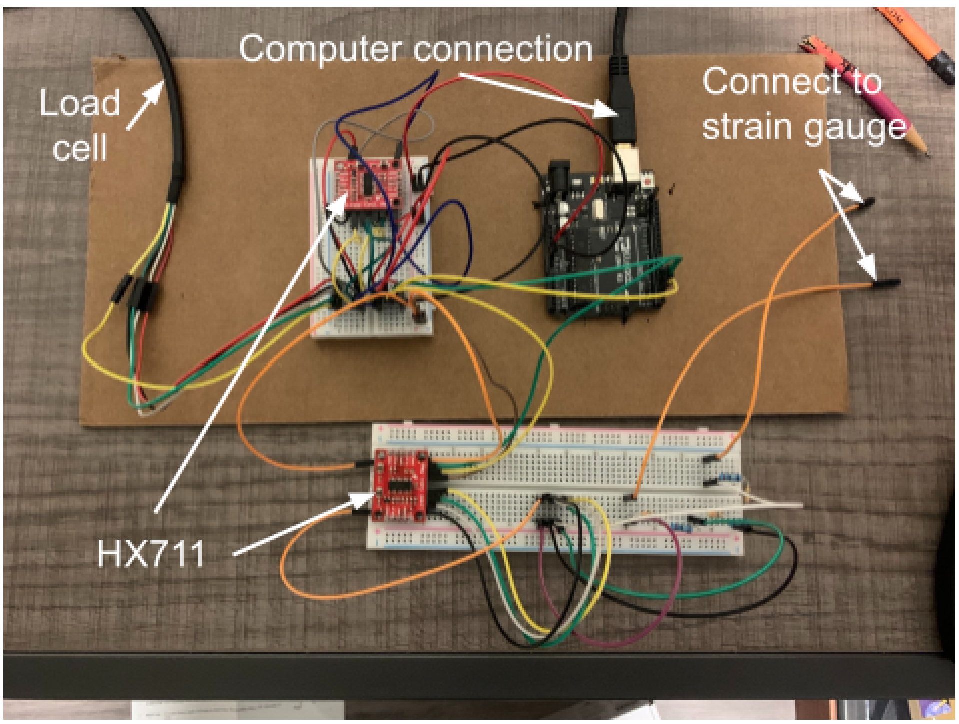

Figure 10. Complete circuit

Our Arduino code read in data from the load cell and strain gauge and outputted values of force in kg (converted to Newtons by multiplying by $g = 9.81\ m/s^2$) and millistrain. An additional program written in Processing outputted the data to a csv file format.

3.5 Experiment/Steps Taken

3.5.1 Experimentation Design

6 pieces were tested for every different test specimen. The first tests completed were control pieces of PLA 3D printed at 100% infill without any damage or repair.

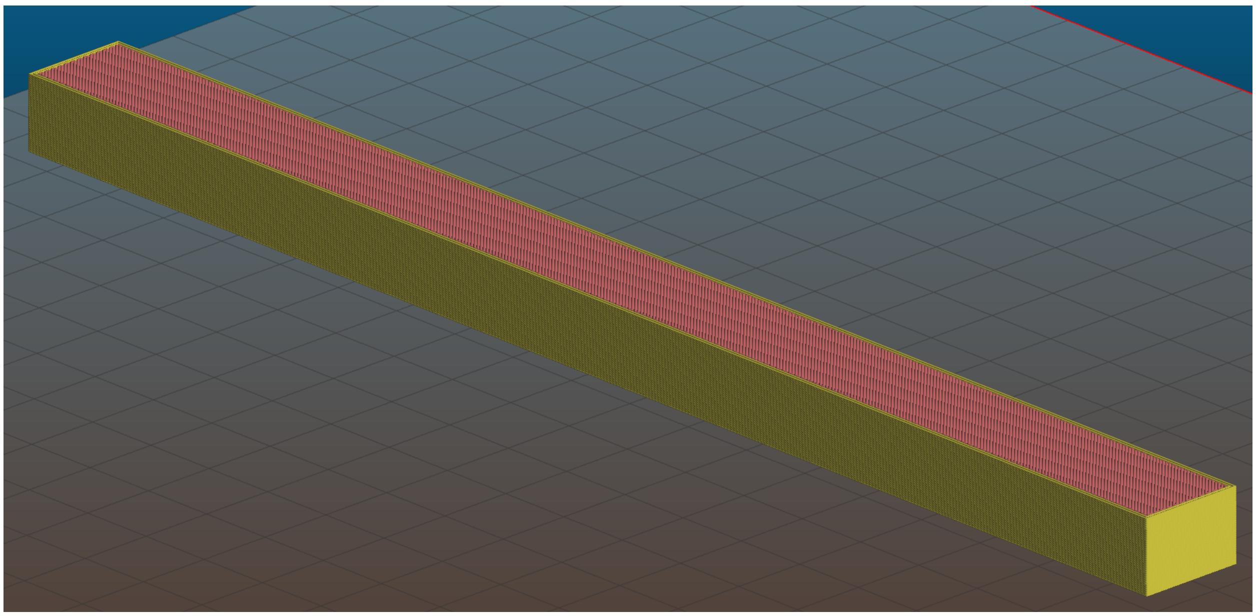

Figure 11. Control piece slicer view

These pieces represented the undamaged structure, and so would be the baseline to which all other testing would be compared. To evaluate the quality of a repair, the ultimate stress and stress vs strain curves were compared between undamaged, damaged, and repaired pieces for a given infill and type of loading (different types of loading are discussed below). Using the load cell, the force applied to the part was measured in kilograms and used to calculate the ultimate strength of the part before failure. The strain of the part was measured in millistrains to ideally note strain at the point of failure. The units of kilograms and millistrains were chosen because these were the units listed in the documentation that came with the sensors.

Control testing was followed by testing of the T1 damaged geometry. The results of this testing were meant to show how much the overall strength of the piece was impacted by a small area of simulated damage. Once again, they would also be compared to the results of the repair testing so we could quantify the impact of the repair on the strength of the overall piece.

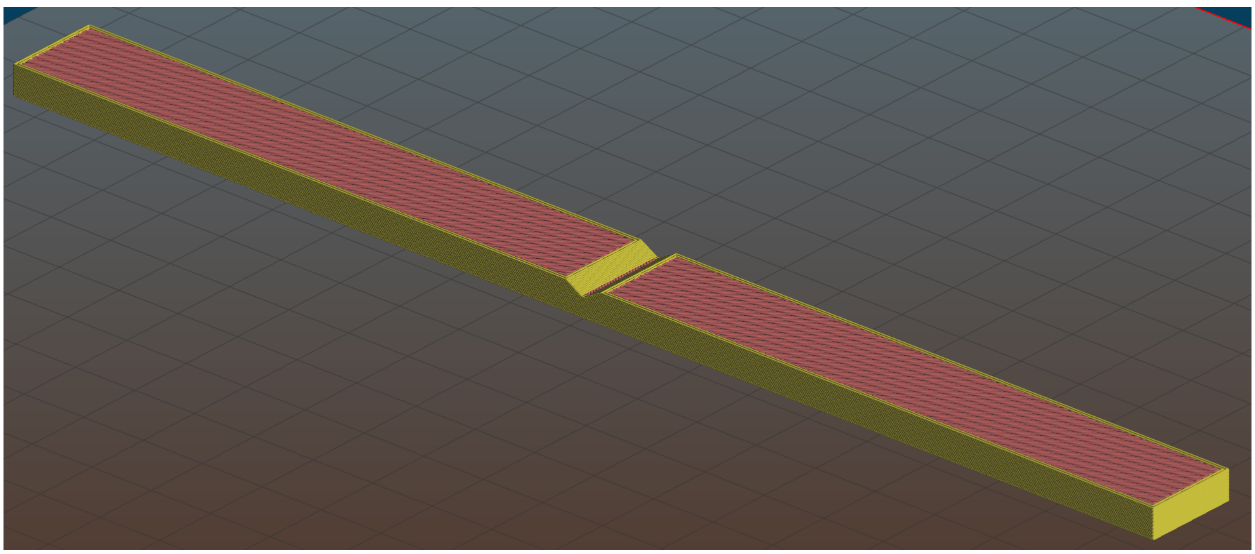

Figure 12. T1 damaged piece slicer view

The infills used for repairs were 20, 40, 60, 80, and 100% while the damaged initial part was kept at 100% for all tests. The repair also used two initial conformal layers that conformed to the geometry of the damage.

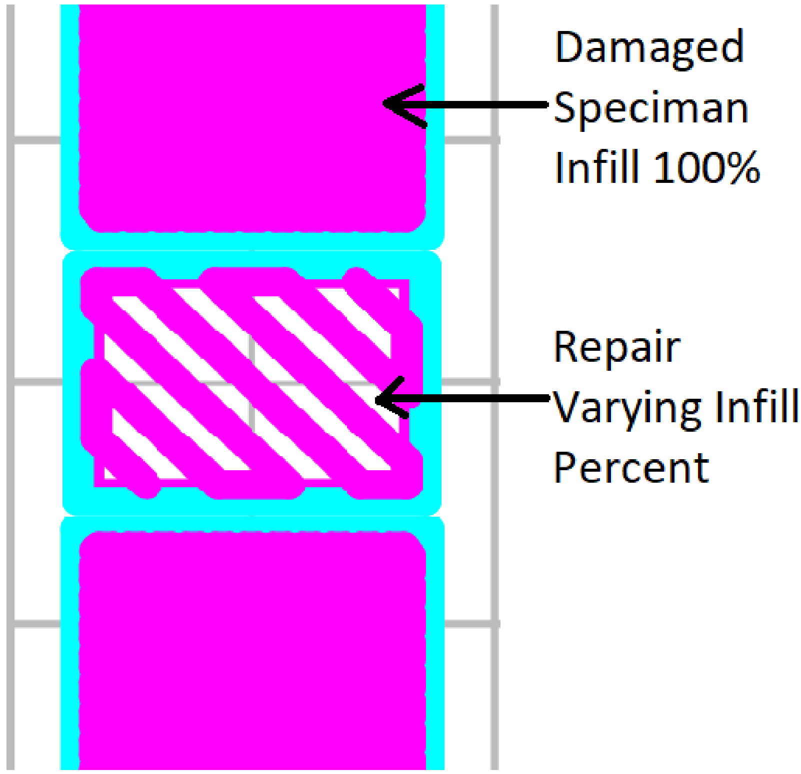

Figure 13. Depiction of infill piece orientation

We wanted to test various infills for the repair to determine which infill would give the maximum ultimate strength and if there was an optimum point for strength vs print time.

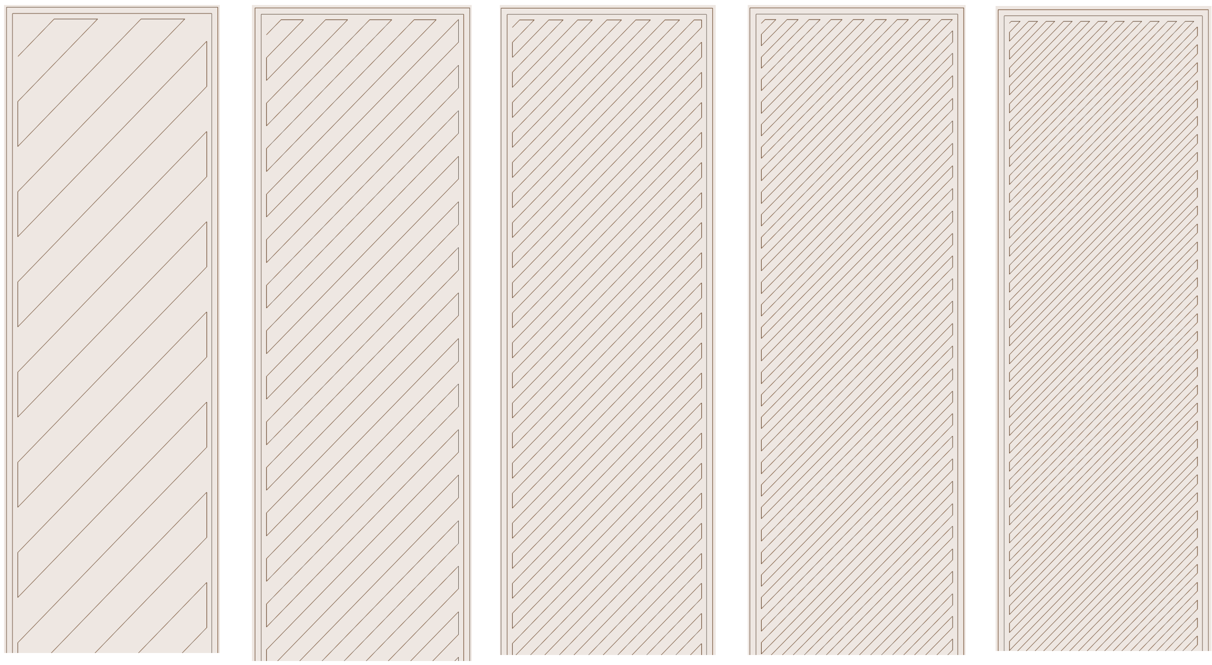

20% Infill 40% Infill 60% Infill 80% Infill 100% Infill

Figure 14. Comparison of toolpath for different infill percentages

After initial infill testing, we wanted to corroborate our results with those of a different damage geometry. Real-life damage comes in an infinite number of sizes and irregular shapes, so to prove that our results are applicable to some general damage with our focused scope, we conducted damaged and repaired testing for the T4 geometry which has rounded instead of flat faces and has a smaller void volume. Our goal here was to be able to show similar trends in the analysis of the results between the T1 and T4 geometries. We also kept in mind that seeing differing trends for the different damage geometries would also be useful information.

Tension Vs. Compression	
T1	T4
6 parts printed with conformal repairs facing down at 100% infill (Tension)	6 parts printed with conformal repairs facing down at 100% infill (Tension)
6 parts printed with conformal repairs facing up at 100% infill (Compression)	6 parts printed with conformal repairs facing up at 100% infill (Compression)

Figure 15. Damaged Geometry testing

When a structure is in bending, one side of it is in tension while the other is in compression. All of our testing was done using 3-point bending, and results were analyzed and compared with the damaged and repaired sections on both sides of the structure. Therefore, damaged and repaired pieces were tested with the void/repair either on top of the beam or on the bottom, which will here on be referred to as the compression or tension cases, respectively. The T1 damage geometry did not allow us to test these pieces with the void in compression because the applied force would have been in the void and hence at an angle (figure 16.), so a basic 3-point bend analysis would not have been appropriate. T4 damaged pieces could be tested in compression because the void did not span the entire width of the piece (figure 17.). Data for both tension and compression were collected for all other pieces.

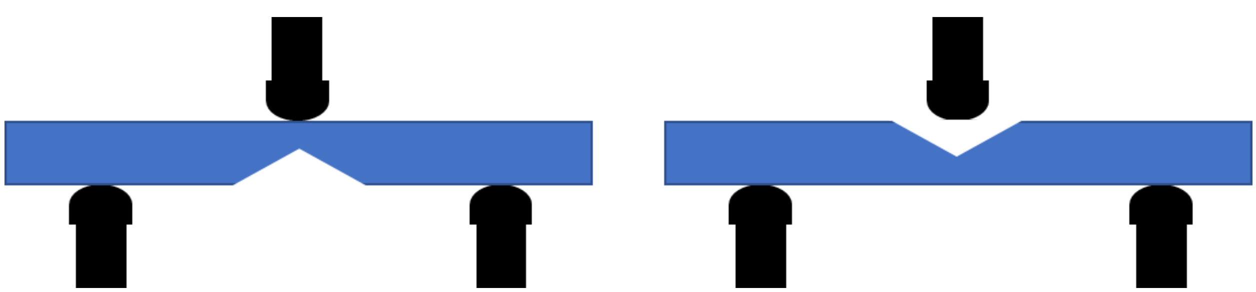

Figure 16. T1 damaged tension testing (Left), T1 damaged compression testing (Right).

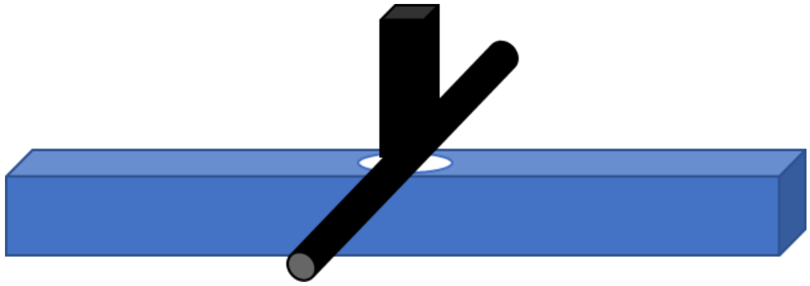

Figure 17. T4 damaged compression testing

Infill Pattern	
Hexagonal	Aligned
12 T1 parts printed at 40% infill (6 compression, 6 tension)	12 T1 parts printed at 40% infill (6 compression, 6 tension)
12 T1 parts printed at 60% infil (6 compression, 6 tension)	12T1 parts printed at 60% infill (6 compression, 6 tension)
12T1 parts printed at 80% infill (6 compression, 6 tension)	12 T1 parts printed at 80% infill (6 compression, 6 tension)

Figure 18. Infill Pattern Testing

The infill pattern used for all testing up to this point was rectilinear. To obtain more comprehensive results, we wanted to vary this as well. The same undamaged (control) and damaged pieces were used as before, and only the infill of the repair itself was varied. The other infill patterns tested were aligned and hexagonal as can be seen above in figure 6, and again the infill percentage was varied between 20, 40, 60, and 80%. (100% infill was not included here because our slicing software and printers were only capable of printing 100% infill in a rectilinear pattern). The results were again obtained for both tension and compression.

Finally, to corroborate our findings and again show that they are applicable to a wider range of cases, we performed T1 infill percentage testing using ABS. Just as when we tested the different damage geometries, we hoped to see similar trends in the analysis between the different materials, but differing behaviors would still be important and useful information.

3.5.2 Printer Setup

To maintain consistency throughout the experimentation process, the team used the Ender Pro 3 with a 0.4mm nozzle and identical settings for each set of prints. The heated printer bed had dimensions of 220 x 220 x 250 mm and a maximum temperature of 110℃. The nozzle and printer bed temperature settings were dependent on the material being used. For PLA prints, the nozzle temperature was set to 200℃ and the bed temperature was 70℃. For ABS prints, the nozzle temperature was set to 200℃ and the bed was set to 95℃.

In addition, the team sprayed a thin layer of hairspray to the printer bed immediately before each piece began printing. This was done to ensure that the first few layers of the print properly adhered to the surface of the bed. Without this step, the initial layers had a tendency to slide across the printer bed, causing the print to fail. In some cases, it was also beneficial to preheat the printer bed for 15-20 minutes before starting the actual print. This improved adhesion to the bed at times when the room temperature was colder than usual; for example, during the winter months or when the air conditioning in the room was set to a lower temperature.

3.5.3 Printing Procedure

A detailed printing procedure was developed to ensure all prints were consistent and the only variables between tests were the actual geometry of the damaged/repaired pieces.

The first step is to preheat the nozzle and bed to specified temperatures as outlined above in section 3.5.2. Afterwards the operator would spray the bed of the 3D printer with hair spray in order to minimize the chance of warping along the edges of the piece. The hairspray added a layer of adhesion between the print bed and the piece being printed. For the purposes of our printing, Suave max hold unscented hairspray was used. If warping continued to be an issue, insulate the 3D printer. This prevents drafts and rapid changes in temperature from causing warping or other complications in our prints. The printers were insulated using cardboard boxes. Figure 19 below shows the following setup.

Figure 19. Insulation of print bed using cardboard

Once all the set up steps were completed the 3D printer printed the base piece. The base piece for every repaired test was a rectangular prism (of dimensions described in Section 3.3: Testing Standards) at 100% infill, with either a T1 or T4 hole in the center of it.

Once the base piece was completed the operator waited at least one hour to allow for the temperature of the nozzle, bed, and PLA to return to standard conditions. This is a crucial step since we are trying to simulate repairing a structure that has already been in operation for some time. If the repair is added before allowing the piece to cool down completely, the resulting piece will be more like one continuous print rather than a conformal print added on to a pre-existing structure.

Finally the operator begins a stopwatch and starts the print of the designated repaired piece. This piece has the correct proportions to fully fill the hole damage of the base piece. Once damage has been completely repaired, stop the stopwatch and record time. For the fill piece, the infill pattern and infill percentage were varied to what was being tested.

3.5.4 Testing Procedure

A detailed testing procedure was developed to ensure all the testing conditions remained consistent, and the only variables between tests were the actual geometry of the damaged/repaired pieces.

The first step is to attach the strain gauge. The strain gauges were attached using super glue onto the underside of each test piece directly underneath the point of applied force (in the middle). A small drop of super glue was applied to the test piece after wiping it clean of any dirt and dust. The strain gauge was then gently applied and the test piece set aside for the glue to sufficiently dry. The strain gauge was placed in the middle so that it would be located at the point of maximum strain and on the underside so that it wouldn't be crushed by the press. This, however, meant that a few of our test geometries could not be tested with a strain gauge applied. When any of the “damaged” pieces, either T1 or T4, were tested in tension (with the void on the bottom), the location that the strain gauge would need to be was exactly where the void in the piece was. Therefore there was no strain data collected for any of the damaged pieces in tension, and analysis was done just using load/stress data.

Next, wires had to be soldered onto the strain gauge. Some strain gauges are available with lead wires already attached, however the ones used did not, and so wires had to be soldered on. The strain gauges are both very small and very fragile, so an accidental tug on a wire could easily tear the strain gauge. Therefore, the test pieces had to be handled very carefully once the wires were attached. It was also important to make sure that the strain gauges did not overheat while applying solder. Too much contact with the soldering iron could burn through or damage the performance of the strain gauge.

Once the strain gauge and wires were attached, the test piece was placed in the testing apparatus. Each test piece was placed on the end supports so that the load cell was positioned directly above the midpoint, and the strain gauge wires were connected to the rest of the Wheatstone bridge circuit.

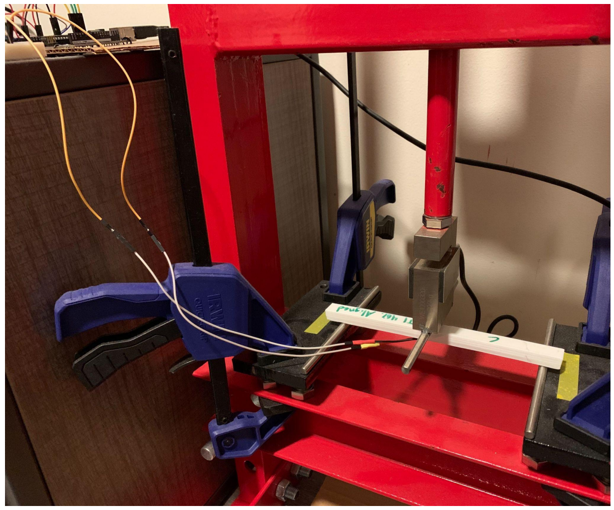

Figure 20. Piece Connected to Arduino and Ready for Testing

With the part in position and the wires connected, the actual test was then run. After zeroing the load cell and editing the Processing code to contain the appropriate test file name, data collection began by running the Processing code. When conducting 3-point bend tests, ASTM standards dictate that the piece must be bent at a rate of 5% strain per second. Since our press was hand-operated in addition to the fact that we could not read in and display strain data as the test was occurring, we were unable to strictly adhere to this standard strain rate. Instead, the press operators simply had to do their best to keep the press rate consistent between tests. Although this deviates from ASTM standards, we do not believe that it had any significant effect on the quality of our data collection or analysis, as we were primarily interested in comparing overall stress vs strain curves as well as maximum stresses.

Each test was run until the piece reached ultimate failure. For some pieces, this was at a clear point when the piece suddenly fractured into two or the repair suddenly snapped off. Other pieces yielded but did not fracture, in which case the test was run until the press reached its maximum stroke. Running the test for longer than necessary was not an issue since the moment of yielding can be easily identified in the data. All data was recorded as csv files with columns of time, force, and strain.

Chapter 4: Results

4.1 Overview

From the conducted experiments, the maximum force applied and the strain at ultimate strength was recorded. In cases where the strain gauge broke before the ultimate strength was achieved, the highest recorded strain was used. From the maximum force applied, the ultimate strength was calculated and both the maximum force and ultimate strength were used for comparison of the efficacy of each repair. Per the ASTM D790 standards, the average force and ultimate strength of the 6 tests for each case were used for the following comparisons. During testing, in most cases, the strain gauge broke before the ultimate strength was reached. Because of this, the strain reached at the ultimate strength of these tests could not be determined and reported.

4.2 Collected Data

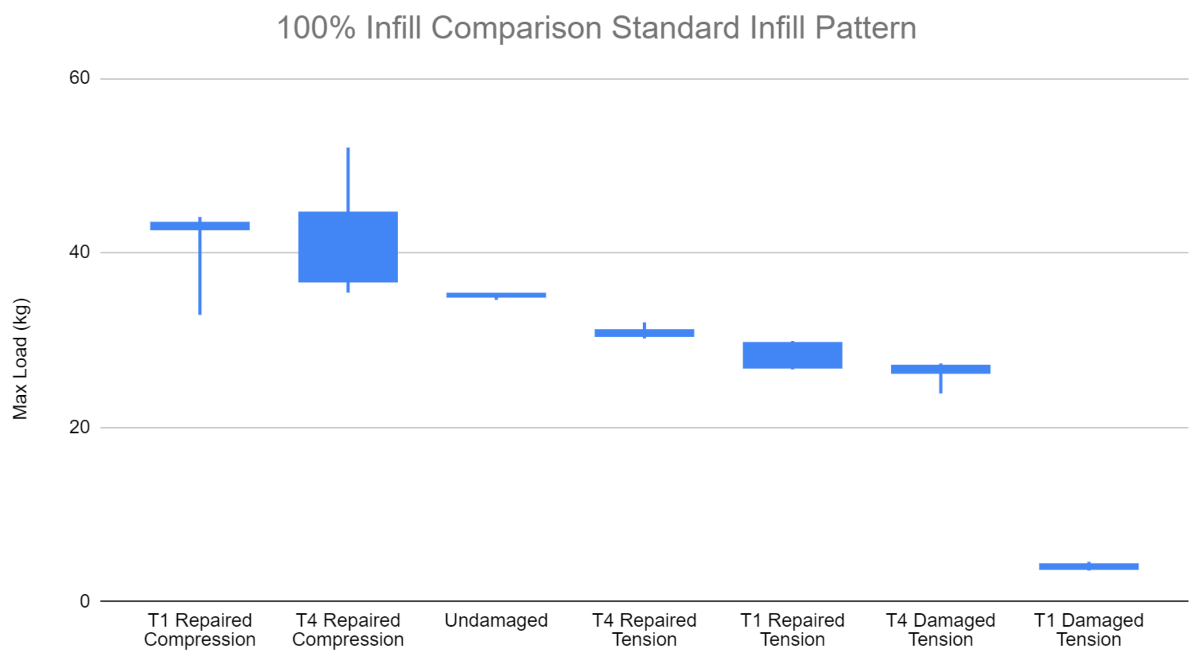

Figure 21. 100% Infill Comparison Standard Infill Pattern

100% Infill Testing				
	Mean Ult. Load (kg)	Std dev. (kg)	Mean Ult. Stress (MPa)	Std dev. (MPA)
T1 Repaired Compression	44	7.22	68	11.33
T4 Repaired Compression	44	8.52	70	13.38
Undamaged	35	0.51	55	0.80
T4 Repaired Tension	31	1.14	49	1.78
T1 Repaired Tension	29	2.04	45	3.20
T4 Damaged Tension	26	1.41	53	2.83
T1 Damaged Tension	4.2	0.53	73	9.23

Figure 22. 100% Infill Testing

For initial 100% infill testing with the rectilinear infill pattern, both the T1 and T4 geometry in compression were found to withstand a higher load than the undamaged control parts. This difference was found to be a 124% and 126% increase respectively in average max strength relative to the undamaged parts. Below the control strength, T4 and T1 repaired pieces in tension were found to have 89% and 82% average strength relative to undamaged with T4 damaged in tension following with 75%. The weakest part of this initial round of testing was found to be T1 damaged in tension with a relative average strength of 12% to undamaged. This testing found that for the T1 and T4 geometries, repairs were effective in increasing strength over damage with compression tests found to be more effective than the undamaged control parts.

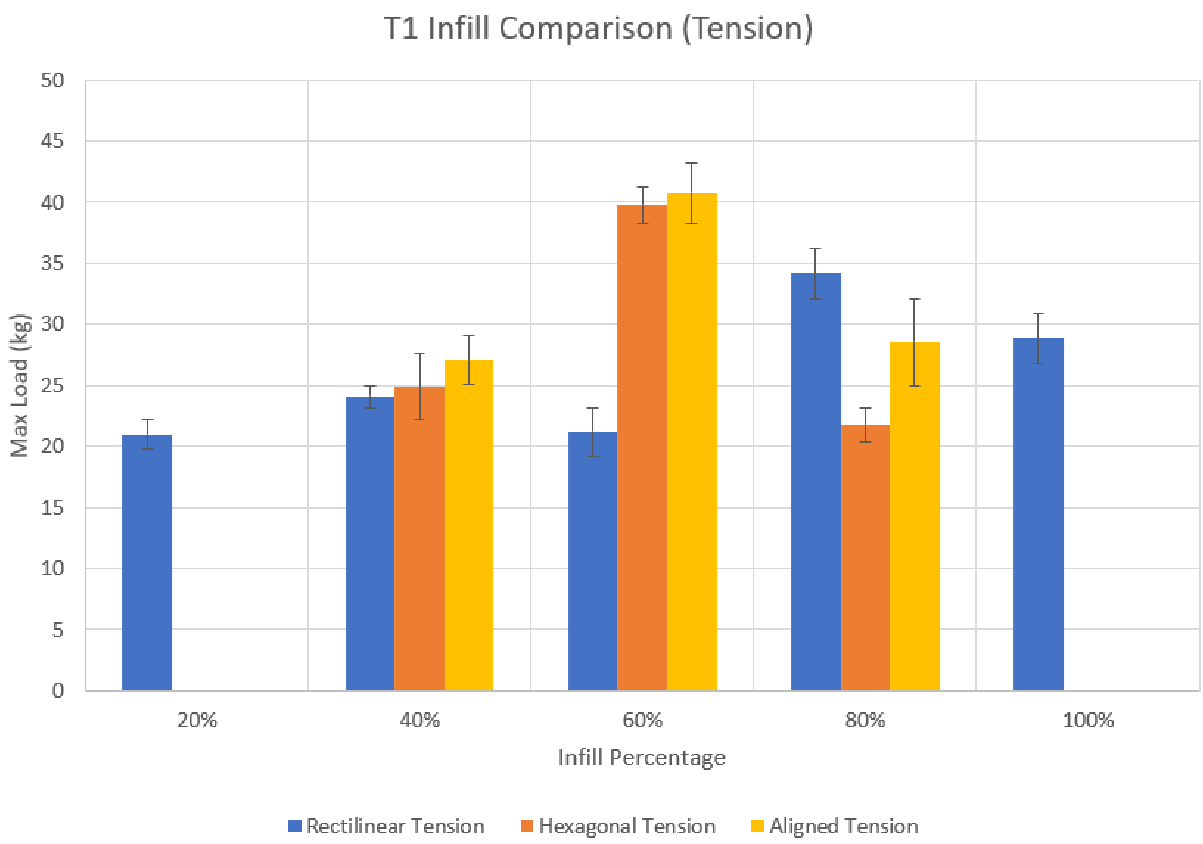

Figure 23. T1 Infill Pattern Tension Testing Graph

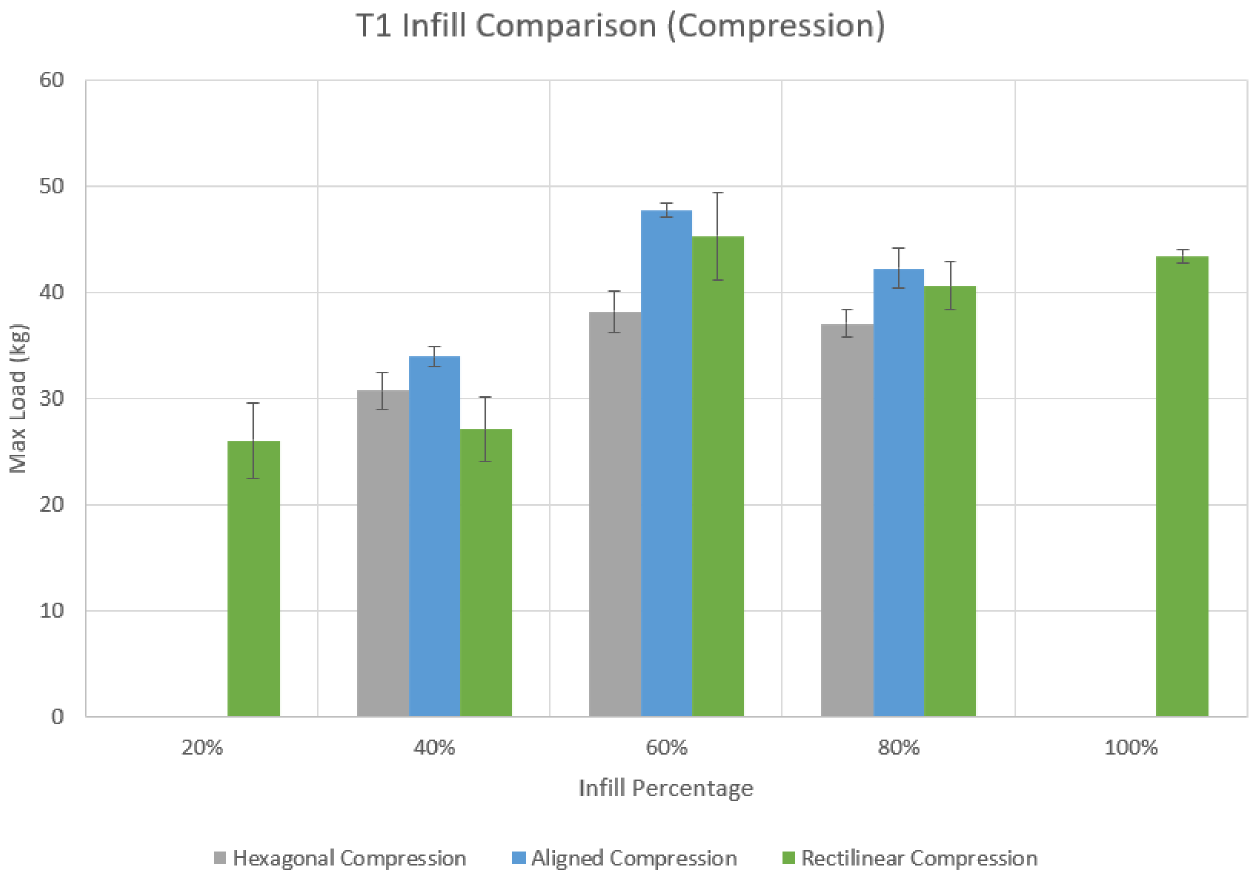

Figure 24. T1 Infill Pattern Compression Testing Graph

T1 Infill Pattern Testing Average Max Load (kg)					
Infill	20%	40%	60%	80%	100%
Rectilinear Tension	21	24	21	34	29
Rectilinear Compression	26	27	45	41	43
Hexagonal Tension		25	40	22	
Hexagonal Compression		31	38	37	
Aligned Tension		27	41	28	
Aligned Compression		34	48	42	

Figure 25. T1 Infill Pattern Testing Data

T1 Infill Pattern Testing Load Relative To Undamaged					
Infill	20%	40%	60%	80%	100%
Rectilinear Tension	63%	72%	64%	103%	87%
Rectilinear Compression	78%	82%	136%	122%	131%
Hexagonal Tension		75%	120%	65%	
Hexagonal Compression		92%	115%	111%	
Aligned Tension		81%	123%	86%	
Aligned Compression		102%	143%	127%	

Figure 26. T1 Infill Pattern Load Relative To Undamaged

From infill pattern testing, the highest mean strengths were found at 60% infill. For tension, the highest load was found with the aligned and hexagonal infills being within each others standard deviations. Under compression, aligned was found to have the highest mean load overall with max load of 48 kg followed closely by rectilinear compression at 45 kg. When compared to the undamaged control tests, at 60% infill all infill patterns under compression and tension were found to be stronger with aligned compression having all 3 infill percentages have over 100% strength.

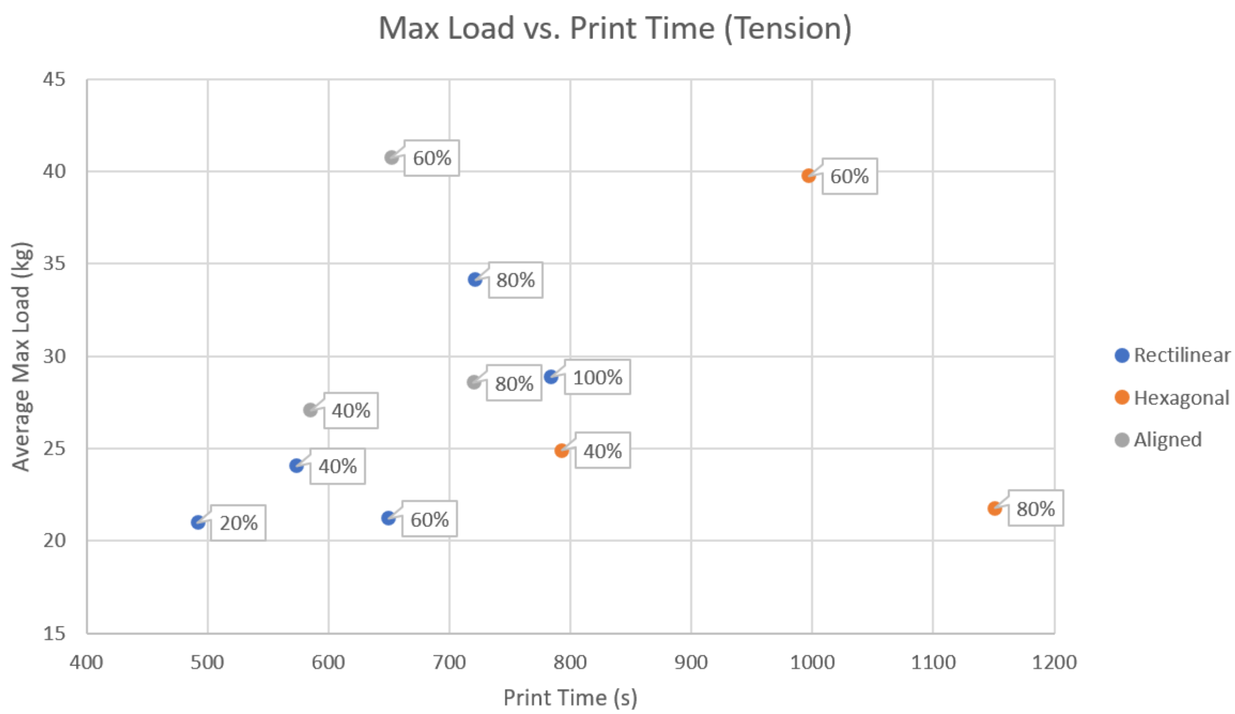

Figure 27. T1 Tension Print Time Vs Max Load Graph

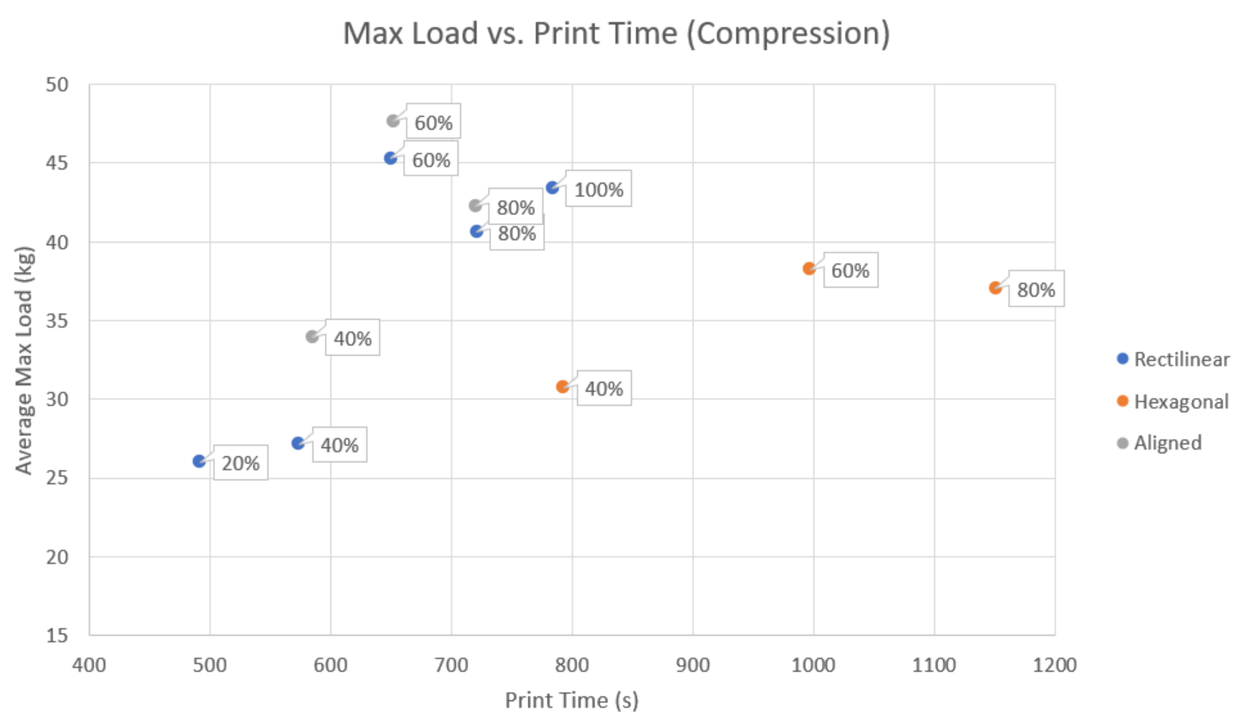

Figure 28. T1 Compression Print Time Vs Max Load Graph

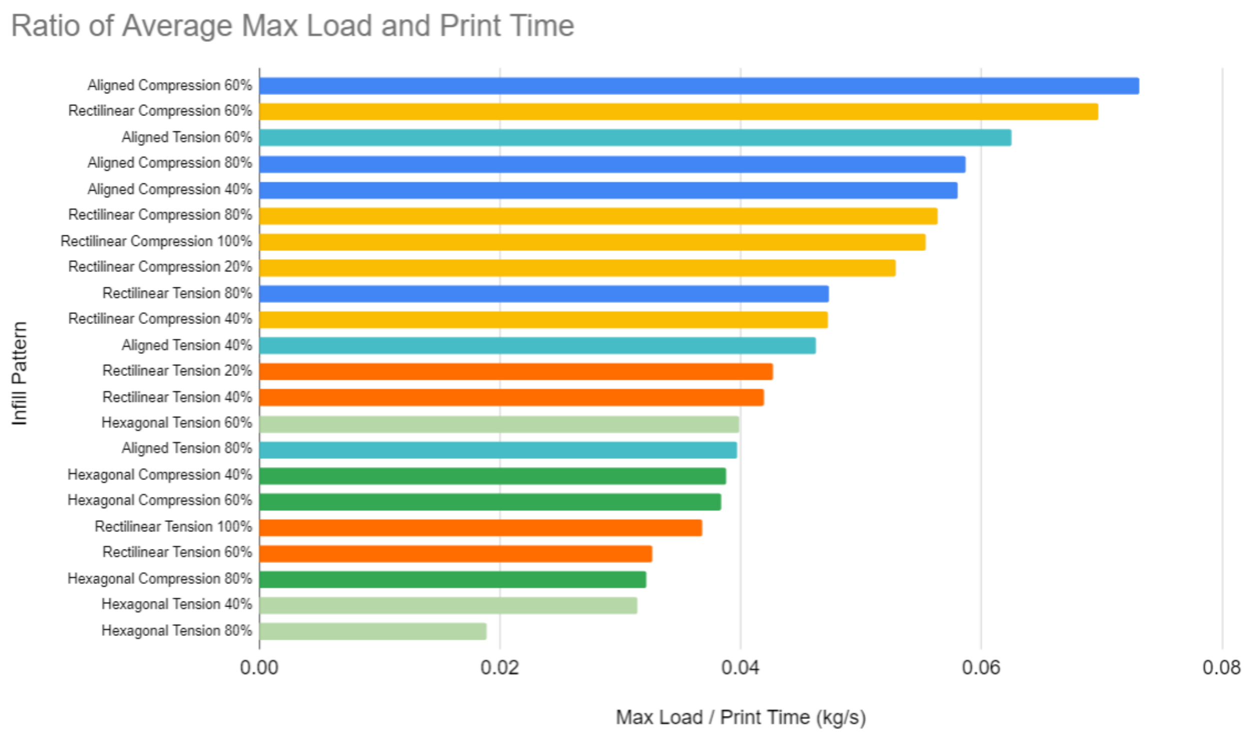

Figure 29. Ratio of Average Max Load against Print Time

The graphs above display the comparison of infill pattern testing results against the time required to print each repair. For both compression and tension, hexagonal had the longest print times at all infills. This was followed by aligned and rectilinear having similar print times for their respective infills. When calculating the ratio of max load and the print times for each infill, the strongest infill from infill pattern testing of aligned at 60% in both compression and tension and rectilinear at 60% in compression were also found to have the best ratio of load against print time. When time is a factor, these infills not only held the most weight, but did not require high print times to be successful.

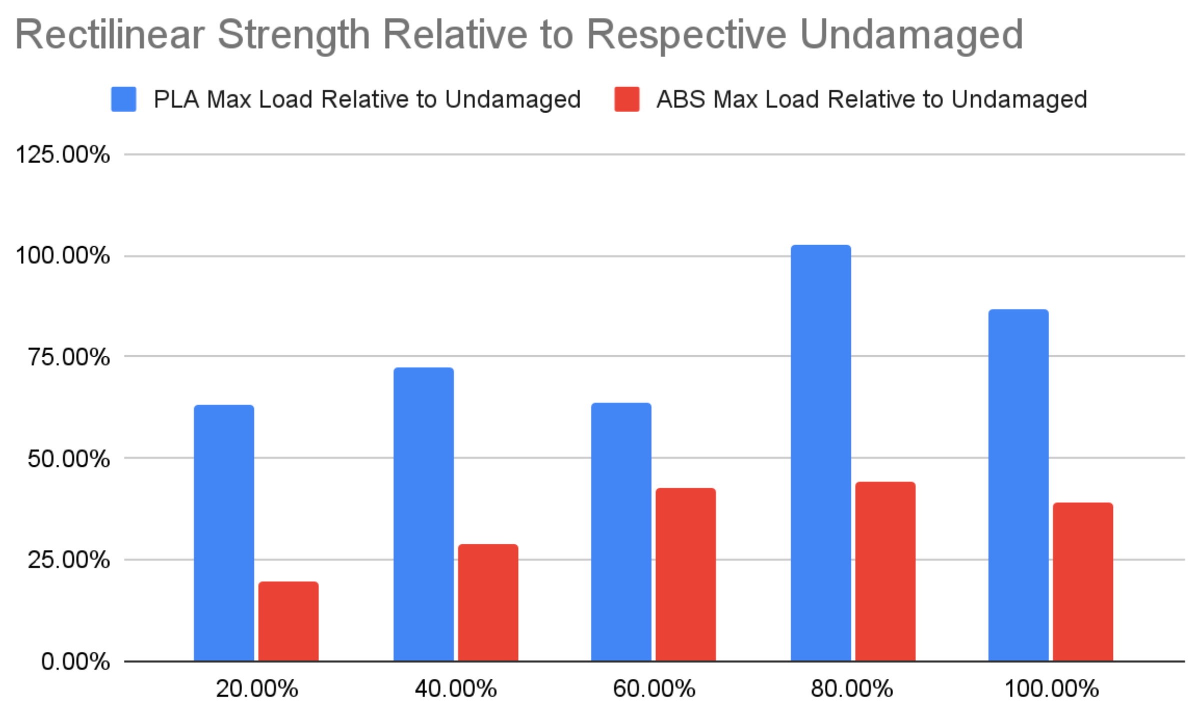

Figure 30. Strength Relative to Respective Undamaged

ABS vs. PLA				
	PLA max Load (kg)	PLA Relative to Undamaged	ABS max Load (kg)	ABS Relative to Undamaged
Undamaged	33		28	
Repaired 100% Infill	29	87%	11	39%
Repaired 80% Infill	34	103%	12	44%
Repaired 60% Infill	21	64%	12	43%
Repaired 40% Infill	24	72%	8	29%
Repaired 20% Infill	21	63%	5	20%
Damaged	4.2	13%	1.5	5%

Figure 31. ABS Vs PLA Testing Data

For the rectilinear ABS testing in comparison to PLA, ABS was found to be much less effective in its repairs than the PLA. The closest ABS repairs were able to reach in comparison to undamaged control was 44% at 80% infill while PLA was able to achieve 103% of the undamaged ultimate strength at 80% infill. This testing does not contradict the earlier findings of the highest mean strength being found at 60% aligned as this testing only consisted of the rectilinear infill pattern.

4.3 Theoretical Analysis

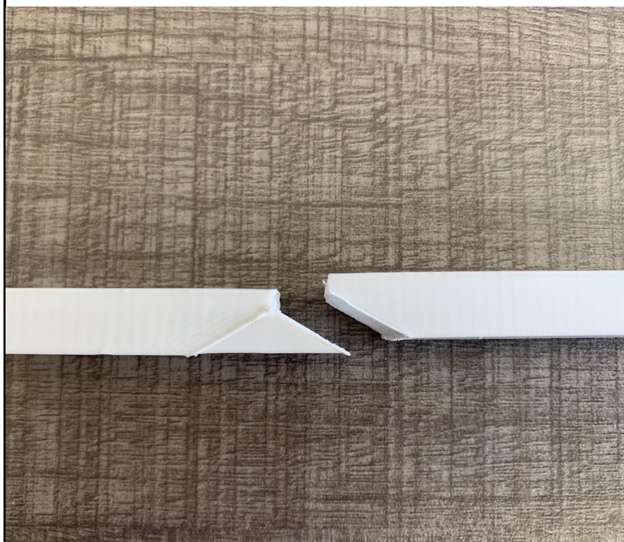	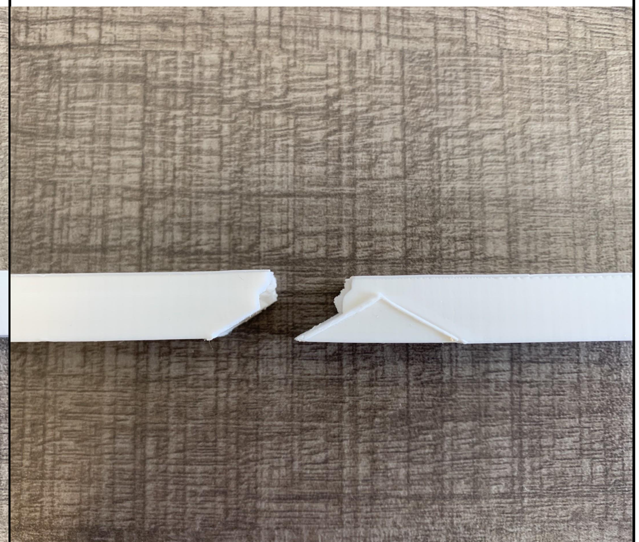
Fracture with repair having infill 100%	Fracture with repair having infill 80%
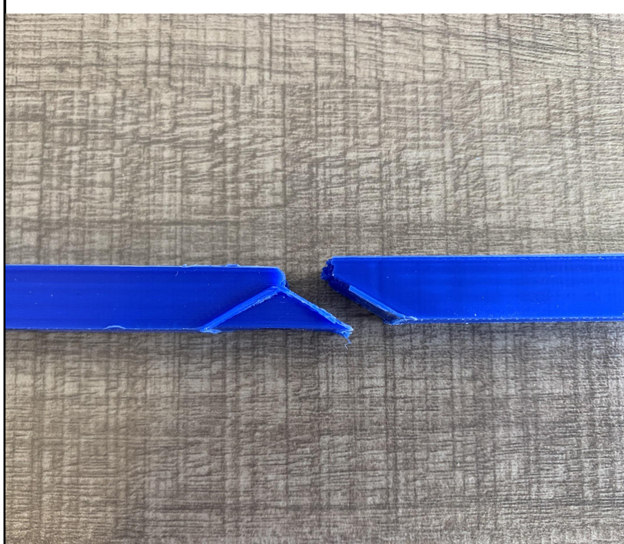	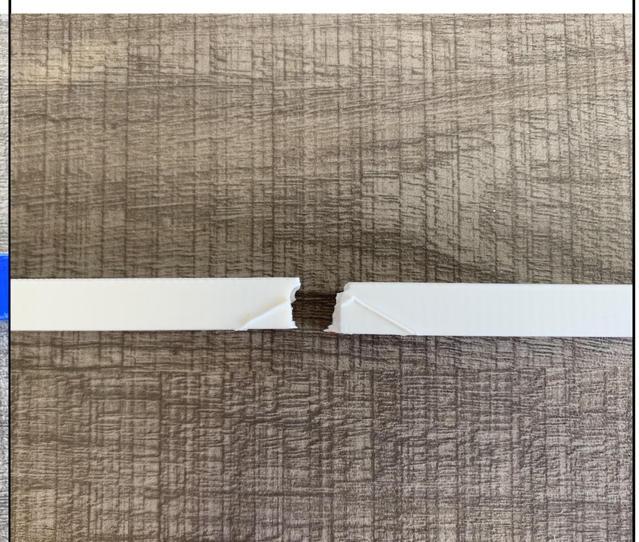
Fracture with repair having infill 60%	Fracture with repair having infill 40%

Figure 32. Fractures at different infills

From our first testing of the T1 samples at different infills, we found the fracture to change as the infill of the repair changed. For 100-60% infill, the fracture is along the repair seam. This changes at 40% infill to break down the middle. For a max force F and length L the internal shear force is F/2 and internal moment is FL/4. For an infinitesimal element along the fracture at the bottom of the test piece (Figure Y, element 1) of the 100-60% infill, it would have the stresses shown in Figure Z.

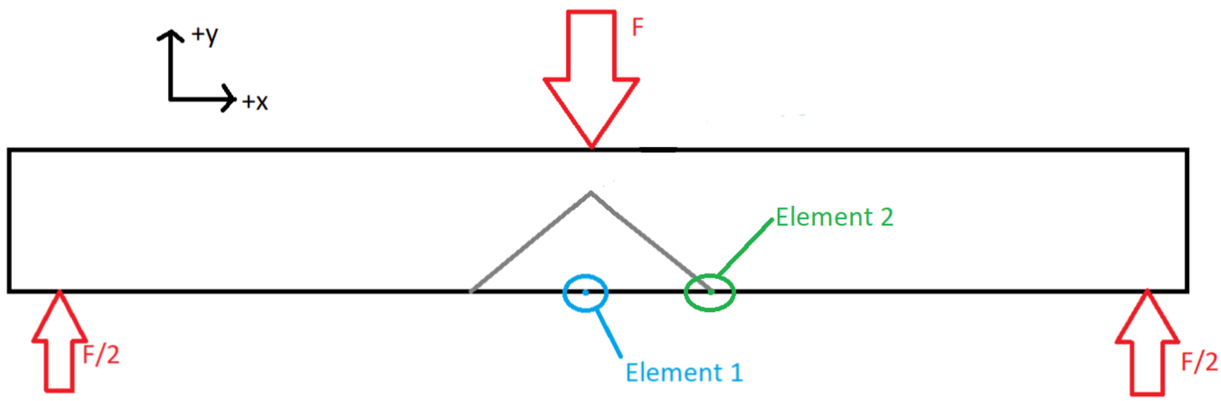

Figure 33. Location of elements on test piece

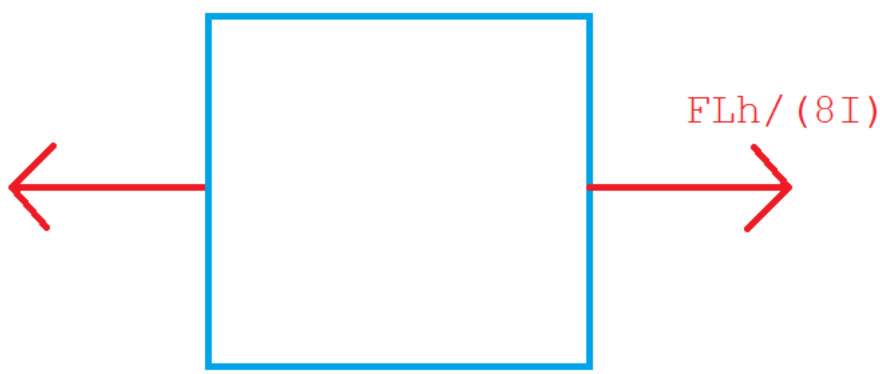

Figure 34. Element 1 Stresses

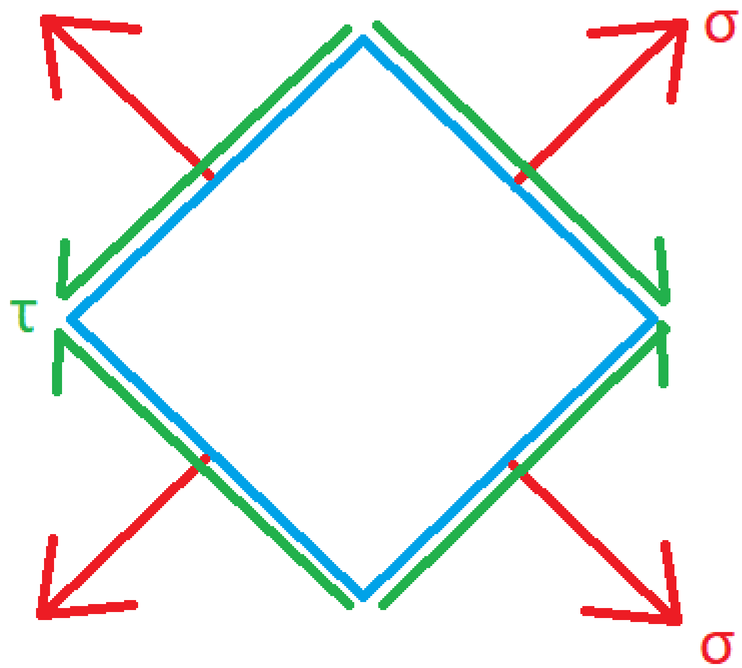

Figure 35. Element 2 Stresses Along Seam

We found that the 60% infill repair actually held less load than the 40% infill repair, and this most likely indicates that the adhesion between the repair and damaged structure has high variability in it's strength that we did not control for. This is apparent from the fact that the seam held up to 14.4MPa shear stress and 14.4MPa normal stress for the 60% repair before failing on average, while the 40% repair held up to 16.3MPa of shear stress and 16.3MPa of normal stress and did not fail. These values are within one standard deviation of each other across our samples. This lets us see the scale of the variability of the adhesion between the damage and the repair. Because of the layout of the repair, changing to orientation of the part during loading places different internal stresses on the repair. Loading the unrepaired side causes the entire part to bend downwards placing tension on the surface connection between the repair and damage. Placing the load on the repair causes the damaged part to compress on the repair at the surface connection. With potential damaged areas having the possibility of placing compression or tension loads on repairs, testing both the effects of different loading on our different tested repairs is necessary to find the best repair for a given scenario.

4.4 Discussion/Conclusion

Four factors were used when determining the optimized solution: infill pattern, infill percentage, print time, and print material. For the infill pattern, the aligned pattern compression was found to be the strongest for the 40, 60, and 80 infill percentages (T1 pattern infill testing graph). rectilinear compression closely followed at 60 and 80 infill percentage as the second highest strength. For the infill percentages, the 60 and 80 had the most outstanding results. The 60 percent infill withstood the highest load when testing with the aligned pattern tension while the rectilinear tension resulted in an obvious low outlier from the remaining patterns' 60 percent infill data. For the rectilinear and hexagonal infill patterns, the 80 percent infill yielded the best results, however they were still lower than the aligned pattern.

In terms of print time, the aligned and rectilinear patterns had similar print times for their respective infills. However, after taking the ratio of max load and print times into consideration, aligned pattern at 60% infill for both compression and tension had the best ratios of load against time, closely followed by rectilinear at 60% in compression. Thus, not only did these infills hold the most weight, but required less time to print as well.

Lastly, in terms of print materials, PLA was much more effective than ABS as the max load of PLA compared to ABS is higher in every percentage of infill for repair (Figure 30.).

Overall, the geometry and infill percentage that gave the best results was the aligned pattern at 60% infill. This was determined through taking the difference between the damaged and repaired data of each of the infill patterns and comparing those differences. Through looking at the data we collected, the aligned pattern gave an increase of 143.37% in effectiveness from the undamaged control piece. Thus, the optimized solution is PLA material with aligned infill pattern at 60% percent infill.

The conducted testing found that nonplanar repairs using a 3D printer were effective in returning strength to damaged pieces with some cases withstanding higher loads than the undamaged control parts. By comparing the variables of infill percentage, infill pattern, and print time for a specific damaged geometry and material, the optimal repair was found based on the maximum load. With further research, these results can be connected to specific situations and conditions to best repair damage.

In a controlled experiment, these results have demonstrated the efficacy of reparative FFF prints. While similar results are expected to hold for other common print materials due to the structural analysis conducted in this section, the testing has empirically confirmed the results for PLA and relatively small voids in beams. In the following section, we will discuss potential weaknesses of our methods and unaddressed research questions stemming from this work.

Chapter 5: Future Work

5.1 Adaptive In-Situ Printing

The objective of this work in combination with scanning is general and adaptive reparative in-situ 3D printing. However, the application of this work has been operating under the assumption that the print location and its topography are known. This is to guarantee that the printer is aware of where exactly to deposit the material required for the repair. General print surfaces that require repair are not necessarily flat nor calibrated with the print head. Knowledge of the local conditions can be computed through a 3D scanning and point-cloud processing procedure. Light Detection and Ranging (LiDAR) is a burgeoning technology whose research advancements make it a natural contender for functioning as this scanner. In consideration for cost efficiency, triangulation scanners offer an inexpensive solution to scanning at shorter distances. This typically would be the case in reparative prints. For example, mounting a triangulation scanner to the manipulator adjacent to the print head would enable close-range scanning to the repair site. Ranging scans are not typically suitable for short-distance as the measurement error is often too large [18]. We would like to consider scanning methods that are on the order of centimeters. When paired with a capable robotic manipulator, this would enable a reasonable range in which both a scan and a print can be made.

General voids or damages are not necessarily flat. In fact, a brief consideration for any type of damage on any type of mechanical structure would likely prompt a disorderly and irregular image. Mounting the print head onto a multiple degree-of-freedom (DOF) robotic manipulator is one way to provide a generic solution. Then, it would be possible for the printer to deposit material in a sequence or in locations that common three-axis printers would not be able to achieve or reach. Using a six DOF manipulator, for example, would allow any print orientation within the robot's workspace. Utilizing more than six may ensure smooth printing due to the avoidance of kinematic singularities (where the solution for the robot's joints are discontinuous as the print head moves along a path).

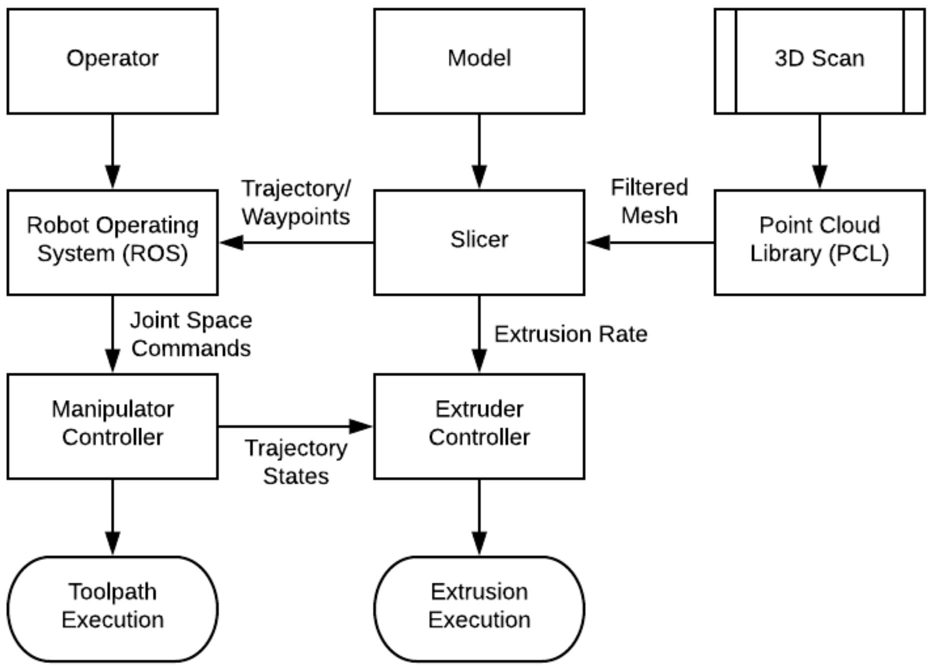

Figure 36. Logical Flow of System Data

Figure 36 represents a high-level design of how such a system would be implemented. Note that a 3D scan can be conducted offline. Scanning and printing do not have to occur sequentially. In the absence of a human expert to ensure that the point cloud produced is sensible, there is greater dependence on the scanning software and data processing reliability.

5.2 Materials

Another area we wanted to study was composite filaments. Unfortunately, due to COVID, we had to readjust our goals midway through our project and decided that it was best to leave composite filaments for future work. Carbon Fiber PLA (CFPLA) is one of the most common reinforced filaments, and future researchers could conduct a very similar procedure to that described above to determine if CFPLA exhibits the similar patterns to PLA and ABS.

The print settings used for effective printing of CFPLA are very similar to that of PLA. The melting point still ranges from 200-230 degrees Celsius, and the bed adhesion will behave similarly to PLA [19]. However, the added fibers in the filament can cause clogging and increasing oozing while printing [19]. Experts recommend using a hardened steel nozzle to prevent damage to the extruder. To prevent clogs from starting to form in the tube, experts also suggest initially reducing the print speed by 25-50% [19]. These tradeoffs must be considered when deciding on a filament to test for our extruder.

CFPLA is a material steadily increasing in popularity due to its increased strength over PLA. There are two types of this material: short fiber reinforced thermoplastics (SFRT) and continuous fiber reinforced thermoplastics (CFRT) [19]. Short fiber reinforced thermoplastics consist of small pieces of carbon fiber embedded in the PLA filament. Continuous fiber reinforced thermoplastics consist of a long strand of carbon fiber embedded into the filament usually during the process of printing.

Future researchers could follow our testing procedures and document their results to compare the strengths vs PLA and ABS. It would be worthwhile to determine if either of these types, SFRT and CFRT, generates higher strengths than the other.

5.3 Extreme Environment

An emerging field that may be able to make use of our research is the commercial space sector. In late 2021, NASA awarded contracts to Blue Origin, Northrop Grumman, and Nanoracks to build a private space station in low Earth orbit (LEO) [20]. With private companies taking a stronghold on this new space race, there will be an increased risk in debris impacts with these large structures. Even with the most advanced debris tracking software at their disposal, sometimes small impacts happen. In May 2021, space debris hit the robotic arm on the International Space Station, leaving a hole in the arm [21]. These smaller objects cannot be tracked with current technology, so although the ISS is able to avoid large debris and satellites, there is always a risk for small collisions. These collisions have the potential to create damaged areas similar to the ones we investigated in our thesis. Below is a test from the European Space Agency of a simulated small debris impact at 15 kilometers per second [22].

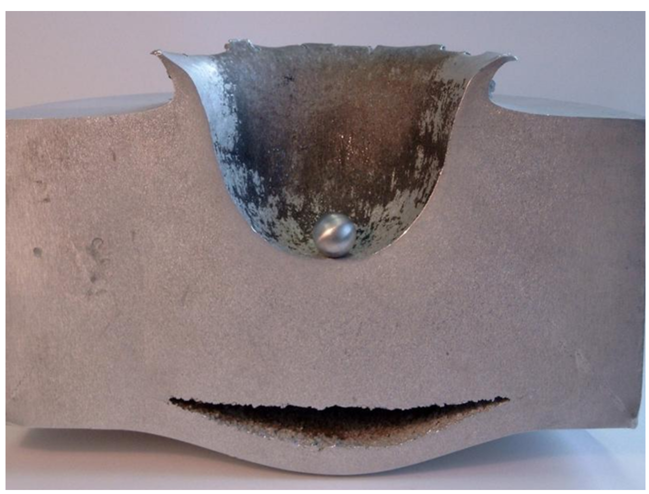

Figure 37. ESA Hypervelocity Impact Test. Image: ESA [22]

Another rapidly increasing source of space debris that has the potential to generate collision events are anti-satellite missile tests. Although these are frowned upon by the scientific community and most space-faring nations, some countries have had a history of demonstrating their capability to destroy satellites in LEO. On November 15th 2021, Russia destroyed one of its old satellites with an anti-satellite missile [23]. According to the Arms Control Association, this single event created over 1500 trackable pieces of space debris that will stay in LEO for years to come [23].

Space debris collision events may require on-orbit servicing for repair. King describes the existing methods of autonomous space servicing and several different robotic systems all designed to carry out various tasks on space stations and satellites [24]. All of the robotic systems described are designed to transport, maneuver, or assemble various objects and payloads [24]. However, none are capable of conducting basic repairs to damaged components. The use of robotics for space servicing is already prevalent, but there is a lack of research and development into a robotic system that could repair damage caused by impact with small pieces of space debris. Such a system could decrease the need for astronauts to risk performing extravehicular activity for basic repairs and may increase the lifespan of satellites and space stations. Future researchers would need to investigate the effect of extreme temperatures on material properties and strength. A similar analysis could be conducted with selective laser melting (SLM) printing to determine the best repair method, and possibly the best repair time. For example, questions to ask could include: would it be better to print in extreme cold or extreme hot? How will these extreme temperature variations affect material properties during and after repair? if a repair is not possible in these conditions, would the printer need to create an artificial environment suitable for repair?

Another area future researchers could study is the microgravity environment and printing. FDM partially relies on gravity to keep layers together as they cool. Other methods of 3D printing applicable to space stations and satellites may have similar challenges in space, which is something researchers would need to address.

Appendix

Equity Report

The overarching goal of our research is to reduce wasted materials by encouraging repair and reuse of damaged components rather than replacement. During our research with Gemstone, we have contributed significant data and analysis to help advance this technology. Additive manufacturing also has great potential for utilizing recycled and/or biodegradable materials. We used PLA to test our proof of concept, which is a material known for being compostable, and is one of the greener polymers to manufacture. With future research into this field, waste made of more complicated materials and in harsher areas can be reduced. Material use would only include the exact amount needed for repair as opposed to complete part replacement of traditional repairs. Previously critical damage could be repaired in situ reducing resources needed for more traditional ex situ repairs.

A future area of research for in-situ 3D printed repairs is the biomedical field. 3D printing in this industry is a growing field, and although this was not the focus of our research, future work can investigate the feasibility of biomedical applications. In situ repairs on structures such as bones will allow for repairs to be further customized to a patients needs and dimensions. Populations with bone damage and defects could benefit from increased accurcary in customized repairs. Our research could be used to advance the medical 3D printing industry.

Processing Code for Press Data Collection

```
//import the required libraries
```

```
import processing.serial.*;

Serial mySerial;
Table table;
String filename;

void setup()
{
  //set mySerial to listen on COM port 10 at 9600 baud
  mySerial = new Serial(this, "/dev/cu.usbmodem141201", 115200);

  table = new Table();
  table.addColumn("Test Time (s)");
  //add a column header "Data" for the collected data
  table.addColumn("F(kg)");
  table.addColumn("millistrain");
}

void draw()
{
  //variables called each time a new data entry is received
  int mili = millis();

  if(mySerial.available())
  {
            bool interupt = false;

            // Interrupt on keypress
            String buffer = "";
                  while (!interupt){
                  if(mySerial.avaliable()) {
                        char next = mySerial.readChar();
                        if (next == '\n') {
                              interupt = true;
                        } else {
                              buffer.append(next);
                        }
                  }
            }

            //add a new row for each value
            TableRow newRow = table.addRow();
            newRow.setString("Test Time (s)", str(mili/1000.0));

            //place the new row and value under the "Data" column
            newRow.setString("F(kg)",split(buffer,',')[0]);
            newRow.setString("millistrain",split(buffer,',')[1]);
  }
}

void keyPressed()
{
  //variables used for the filename timestamp
  int d = day();
  int m = month();
```

```
  int h = hour();
  int min = minute();
  int s = second();
  // variable as string under the data folder set as (mm-dd--hh-min-s.csv)
  filename = "/Testing Data (GEMS)/U" + "(" + str(m) + "." + str(d) +
")"+str(h)+":"+str(min)+".csv";
  //save as a table in csv format(data/table - data folder name table)
  saveTable(table, filename);
  exit();
}
```

Arduino Code for Press Data Collection

```
#include <HX711.h>

#define DOUT  3 //load cell
#define CLK  2  //load cell
#define DOUT2  4 //strain guage
#define CLK2  5 //strain guage

HX711 scale1;
HX711 scale2;

float force_calibration_factor = -22400;
float strain_calibration_factor = 255612315;

void setup() {
  Serial.begin(115200);
  scale1.begin(DOUT, CLK);
  scale1.set_scale(force_calibration_factor);
  scale1.tare();

  scale2.begin(DOUT2, CLK2, 32);
  scale2.set_scale(strain_calibration_factor);
  scale2.tare();


}

void loop() {
  scale1.set_scale(force_calibration_factor);
  scale2.set_scale(strain_calibration_factor);
  while(!Serial.availableForWrite()){}
  float force = scale1.get_units();
  float r = scale2.get_units();
  Serial.print(scale1.get_units(), 2);
  Serial.print(',');
  Serial.print(scale2.get_units(), 7);
  Serial.println();
}
```

References

[1] Nick Quigley and James Evans Lyne, “Development of a Three-Dimensional Printed, Liquid-Cooled Nozzle for a Hybrid Rocket Motor,” *J. Propuls. Power*, vol. 30, no. 6, pp. 1726–1727, 2014, doi: 10.2514/1.B35455.

[2] Robert M. Taylor *et al.*, “Design Optimization, Fabrication, and Testing of a 3D Printed Aircraft Strucutre Using Fused Deposition Modeling,” *AIAA Scitech 2020 Forum*, 2020. https://doi.org/10.2514/6.2020-1924

[3] Liseli Baich, Guha P. Manogharan, and Hazel Marie, “Study of infill print design on production cost-time of 3D printed ABS parts,” *Int. J. Rapid Manuf.*, vol. 5, no. 3, p. 308, doi: 10.1504/IJRAPIDM.2015.074809.

[4] M. Doran, R. Sterritt, and G. Wilkie, “Autonomic Self-Adaptive Robot Wheel Alignment,” in *Adaptive 2016: The Eighth International Conference on Adaptive and Self-Adaptive Systems and Applications*, 2016, pp. 27–33.

[5] S. Siceloff, “Meet The ‘Swarmies’- Robotics Answer to Bugs,” *NASA*, Mar. 02, 2015. http://www.nasa.gov/content/meet-the-swarmies-robotics-answer-to-bugs (accessed Oct. 16, 2019).

[6] “NASA/JPL-Caltech/MSSS; Sol 962, April 21, 2015.” https://mars.jpl.nasa.gov/msl-raw-images/msss/00962/mcam/0962ML0042560020403852E01_DXXX.jpg (accessed Oct. 23, 2019).

[7] P. Hanaphy, “Saab Trials 3D Printing to Repair Battle-Damaged Gripen Fighter Aircraft.” [Online]. Available: https://3dprintingindustry.com/news/saab-trials-3d-printing-to-repair-battle-damaged-gripen-fighter-aircraft-187974/

[8] S. Farah, D. Anderson, and R. Langer, “Physical and Mechanical Properties of PLA, and Their Functions In Widespread Applications -- A Comprehensive Review,” *Adv. Drug Deliv. Rev.*, vol. 107, pp. 367–92, Dec. 2016.

[9] “A Detailed Guide on Acrylonitrile Butadiene Styrene,” *Omnexus The material science platform*. https://omnexus.specialchem.com/selection-guide/acrylonitrile-butadiene-styrene-abs-plastic

[10] “Elongation at Break,” *Omnexus The material science platform*. https://omnexus.specialchem.com/polymer-properties/properties/elongation-at-break

[11] C. Abeykoon, P. Sri-Amphorn, and A. Fernando, “Optimization of fused deposition modeling parameters for improved PLA and ABS 3D printed structures,” *Int. J. Lightweight Mater. Manuf.*, vol. 3, no. 3, pp. 284–297, Sep. 2020.

[12] F. Alkadi and K.-C. Lee, “Conformal additive manufacturing using a direct-print process”.

[13] “(PDF) ,” *ResearchGate*.

https://www.researchgate.net/publication/335542750_3D_Printing_of_Nonplanar_Layers_for_Smooth_Surface_Generation (accessed Sep. 03, 2020).
[14] H. Tanner, "Observing the effect of infill shapes on the tensile characteristics of 3D printed plastic parts," Wichita State University, 2016. [Online]. Available: http://hdl.handle.net/10057/13504
[15] S. Khan, H. Zakaria, Y.L.Chong, M. A. M. Saad, and K. Basaruddin, "Effect of infill on tensile and flexural strength of 3D printed PLA parts," in *IOP Conference Series: Materials Science and Engineering*, 2018, vol. 429. doi: :10.1088/1757-899X/429/1/012101.
[16] M. Kamaal, M. Anas, H. Rastogi, and N. Bhardwaj, "Effect of FDM process parameters on mechanical properties of 3D-printed carbon fibre–PLA composite," *Prog. Addit. Manuf.*, vol. 6, pp. 63–69, Aug. 2020.
[17] "Standard Test methods for flexural properties of unreinforced and reinforced plastics and electrical insulating materials," *Annu. Book ASTM Stand.*, vol. 8, no. 1, 2017.
[18] J. G. D. M. Franca, M. A. Gazziro, A. N. Ide, and J. H. Saito, "A 3D scanning system based on laser triangulation and variable field of view," in *IEEE International Conference on Image Processing 2005*, Sep. 2005, vol. 1, p. I–425. doi: 10.1109/ICIP.2005.1529778.
[19] M. Heidari-Rarani, M. Rafiee-Afarani, and A. M. Zahedi, "Mechanical characterization of FDM 3D printing of continuous carbon fiber reinforced PLA composites," *Compos. Part B Eng.*, vol. 175, p. 107147, Oct. 2019, doi: 10.1016/j.compositesb.2019.107147.
[20] M. Sheetz, "NASA awards Blue Origin, Northrop Grumman and Nanoracks with contracts to build private space stations," *CNBC*, Dec. 02, 2021. https://www.cnbc.com/2021/12/02/nasa-private-space-station-contracts-blue-origin-nanoracks-northrop.html (accessed Feb. 14, 2022).
[21] "Space junk slams into International Space Station, leaving hole in robotic arm." https://www.cbsnews.com/news/space-junk-damage-international-space-station/ (accessed Feb. 14, 2022).
[22] "Hypervelocity impacts and protecting spacecraft." https://www.esa.int/Safety_Security/Space_Debris/Hypervelocity_impacts_and_protecting_spacecraft (accessed Feb. 14, 2022).
[23] "Russian ASAT Test Creates Massive Debris | Arms Control Association." https://www.armscontrol.org/act/2021-12/news/russian-asat-test-creates-massive-debris (accessed Feb. 14, 2022).
[24] D. King, "SPACE SERVICING: PAST, PRESENT AND FUTURE," 2001.